



Combined loadings after medium velocity impact on large CFRP laminated plates: Discrete ply model simulations

Joel Serra, A Trelu, Christophe Bouvet, Samuel Rivallant, Bruno Castanié, L
Ratsifandrihana

► To cite this version:

Joel Serra, A Trelu, Christophe Bouvet, Samuel Rivallant, Bruno Castanié, et al.. Combined loadings after medium velocity impact on large CFRP laminated plates: Discrete ply model simulations. Composites Part C: Open Access, 2021, 6, <10.1016/j.jcomc.2021.100203>. <hal-03512437>

HAL Id: hal-03512437

<https://hal.science/hal-03512437v1>

Submitted on 5 Jan 2022

HAL is a multi-disciplinary open access archive for the deposit and dissemination of scientific research documents, whether they are published or not. The documents may come from teaching and research institutions in France or abroad, or from public or private research centers.

L'archive ouverte pluridisciplinaire **HAL**, est destinée au dépôt et à la diffusion de documents scientifiques de niveau recherche, publiés ou non, émanant des établissements d'enseignement et de recherche français ou étrangers, des laboratoires publics ou privés.



HAL Authorization

Combined loadings after medium velocity impact on large CFRP laminated plates: Discrete ply model simulations

J. Serra , A. Trelu , C. Bouvet , S. Rivallant , B. Castanié ,
L. Ratsifandrihana

PII: S2666-6820(21)00096-7
DOI: <https://doi.org/10.1016/j.jcomc.2021.100203>
Reference: JCOMC 100203



To appear in: *Composites Part C: Open Access*

Received date: 17 June 2021
Revised date: 20 October 2021
Accepted date: 28 October 2021

Please cite this article as: J. Serra , A. Trelu , C. Bouvet , S. Rivallant , B. Castanié , L. Ratsifandrihana , Combined loadings after medium velocity impact on large CFRP laminated plates: Discrete ply model simulations, *Composites Part C: Open Access* (2021), doi: <https://doi.org/10.1016/j.jcomc.2021.100203>

This is a PDF file of an article that has undergone enhancements after acceptance, such as the addition of a cover page and metadata, and formatting for readability, but it is not yet the definitive version of record. This version will undergo additional copyediting, typesetting and review before it is published in its final form, but we are providing this version to give early visibility of the article. Please note that, during the production process, errors may be discovered which could affect the content, and all legal disclaimers that apply to the journal pertain.

© 2021 Published by Elsevier B.V.
This is an open access article under the CC BY-NC-ND license
(<http://creativecommons.org/licenses/by-nc-nd/4.0/>)

Combined loadings after medium velocity impact on
large CFRP laminated plates: Discrete ply model simulations

J. Serra^{1*}, A. Trellu^{1,2}, C. Bouvet¹, S. Rivallant¹, B. Castanié¹ and L. Ratsifandrihana²

¹*Université de Toulouse, Institut Clément Ader (UMR CNRS 5312), ISAE-*

SUPAERO/UPS/IMT Mines Albi/INSA Toulouse

10 av. E. Belin, 31055 Toulouse, FRANCE

²*SEGULA Aerospace and Defence*

24 bd. Déodat de Severac, 31770 Colomiers, France

**Corresponding author:*

Joel Serra, joel.serra@isae-supaeero.fr

5 Boulevard Richard Wagner, 31300 Toulouse, France

Keywords: *Composite structures, Structural testing, Medium velocity impact, Combined loading, Numerical modeling*

Abstract

To decrease development costs of aeronautical composite structures, industrials and academic researchers are turning to “virtual testing” methods. To help achieve this objective, a new methodology has been developed at the Institut Clément Ader. It is based on a complex loading test rig for technological specimens (more representative than the usual level of coupons) and the Discrete Ply Model (DPM), a model allowing the main damage occurring in composite structures to be simulated. This research focuses on the combined loading of CFRP plates after impact. In a previous work, plates were

experimentally impacted and loaded after the impact in the VERTEX test rig and a methodology to transfer boundary conditions to the numerical model was validated using a simple model without damage. In the work presented here, the DPM was used to simulate both the impact and the complex loading after impact tests. Numerical results and experimental results showed satisfactory correlation. The research undertaken demonstrates that the impact damage has very little influence when the tests are performed at larger scales than coupons. It is therefore paramount to use a pyramidal approach to design and test composite structures, in order to avoid oversizing.

1. Introduction

Composites present high mechanical properties and are now widely used in aeronautical structures but they are sensitive to low velocity impacts. These impacts, due to unexpected dropping of tools during aircraft ground operations or the presence of small debris on the landing area [1], for example, can significantly reduce the residual strength of the structure even if the damage is not visible (Figure 1). The residual compression strength after impact is the most critically affected due to the buckling of delaminated plies [3-4] and can fall by 50% [5-6]. This impact damage issue imposes a damage tolerance approach in the design of composite structures in order to ensure that the structure will withstand in-service loads even if the damage is undetectable. This design philosophy has led to standards for composite coupons under low velocity impact [7] and compression after impact [8].

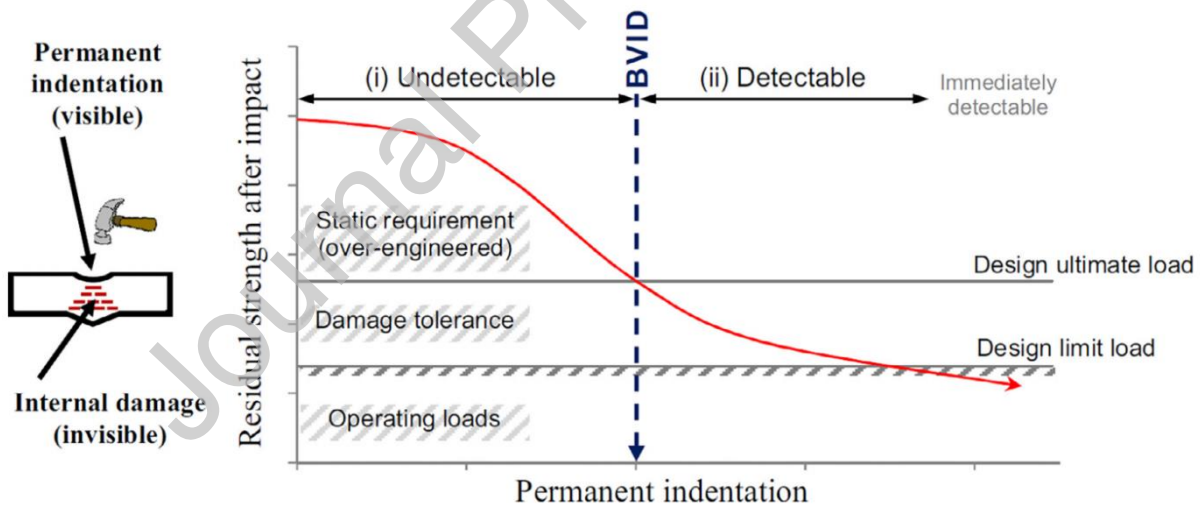


Figure 1: Damage tolerance concept with detectable and undetectable damage [2]

1.1. Simulation of failure in composites

The complex failure phenomena affecting composites depend on several parameters, such as the stacking sequence, the nature of the fibers, the ply thickness, etc., and thus prohibit the use of analytical or semi-analytical models [3, 9-13] alone in the design of structures subject to low velocity impact. These methods are coupled with experimental campaigns following the pyramid of tests design philosophy [14]. To replace these long and costly experimental campaigns (tens of thousands of tests per aircraft), numerical simulations based on the Finite Element (FE) method are being developed and can simulate damage occurring during low velocity impact and compression after impact. This is the “Virtual Testing” approach [15].

The main damage occurring within the ply (intra-laminar) during a low velocity impact is matrix cracking and fiber breakage. In addition, delamination can develop between two plies (inter-laminar) [16-19]. Fiber breakage and delamination are the most critical types of damage for laminate failure. These two failures decrease the laminate stiffness [3, 20] as broken fibers cannot absorb forces and delamination principally reduces compression and bending resistance. Even if very low velocity impacts do not induce fiber failures, the delamination can lead to strongly decreased structural efficiency [21-22]. Matrix cracking is not critical for the safety of a structure but is the first damage occurring during an impact [3, 23] and plays an important role in the impact damage scenario. Bending of the global structure induces tension in bottom plies, which leads to matrix cracking. These cracks propagate into the ply thickness and create delamination when they meet a ply with a different orientation. It is therefore important to represent these three main types of damage (fiber failure, matrix cracking and delamination) and their coupling efficiently. Various methods to model such interlaminar and intralaminar damage have been described.

- Interlaminar (delamination): The literature principally mentions three different methods to simulate delamination. The Virtual Crack Closure Technique (VCCT) was introduced by Krueger [24] and, in particular, used by Li et al. [25] to propagate an existing crack node by node, comparing the energy required to close the crack to the material tenacity. However, the VCCT suffers from some difficulties: it can only simulate the crack propagation and requires topological information from nodes ahead and behind the crack front to calculate the energy required to close the crack. This need for nodal information involves a remeshing for crack propagation. The Cohesive Zone Model (CZM), introduced by Dugdale [26] and Barenblatt [27], has been used to create cohesive interface elements located in a crack zone. The use of CZM involves knowing the crack location, which is not a problem with laminates because delamination appears between plies with different orientations. Cohesive interface elements can predict both crack initiation and propagation. The CZM is widely used in the literature to simulate delamination occurring during low velocity impact [17, 28-31]. Studies of cohesive parameters, such as interface stiffness and mesh size effects, to ensure good delamination behavior are proposed in the literature [32-33] and lead to the conclusion that a short cohesive zone enables better results. Menna et al. have employed 3D elements to represent laminate plies and model delamination by using a contact “surface-to-surface tiebreak” between any two plies [19]. The contact is driven by interface strength parameters. This third method is used but is not as common as cohesive interfaces. It has the advantage of not needing coincident meshes for plies.
- Intralaminar (matrix cracking and fiber breakage): intralaminar damage modeling is most often based on continuum damage theories. Damage is not represented

geometrically and kinematically; only its effect on the mechanical properties is taken into account. When an initiation criterion is reached, the laminate stiffness is degraded in the direction considered until failure occurs. Several researchers [16-17, 34-36] have used the continuum damage model approach to simulate both matrix cracking and fiber breakage in 3D elements with a non-oriented mesh. However the limit of this method concerning damage locations should be underlined: the model response is strongly dependent on the mesh size. To overcome this issue, Pinho et al. [38] and Bouvet et al. [39] simulated the fiber failure by dissipating a surface energy that is independent of the mesh size, as introduced by Bazant & Oh [37]. Another way to represent the matrix cracking is to use cohesive elements in the ply thickness between 3D elements oriented in the fiber direction. This method has been used by several researchers [17, 40-41] who assume that the matrix cracking location is known. Moura et al. [40] place cohesive elements where matrix cracking is observed experimentally and Leopold & Harder study the relation between ply thickness and the distance between two instances of matrix cracking [42].

Because matrix cracking plays an important role in the occurrence of delamination, the importance of the coupling between interlaminar and intralaminar damage in composite laminates is well accepted in the literature [17, 22, 43-45]. The use of cohesive elements in the ply thickness and between plies allows the coupling between these two types of damage to be captured well and thus gives good results in low velocity impact simulation.

To estimate the residual strength in compression after impact and evaluate the damage tolerance of the laminate, some models simulate both low velocity impact and compression after impact on Abaqus/Explicit [22, 46-49] and on Abaqus/Implicit [50].

1.2. About Multiaxial testing

As detailed by Trellu et al. [51], only a few test rigs in the world allow structural details to be tested with multiaxial loading. The state of the art concerning this kind of multiaxial test rigs can be found in [52-53]. Two families of machines are described. In the first, actuators directly reproduce the compression/shear loads on a square meter specimen [54-57]. These test rigs look technically complex, with the use of many actuators to obtain compression/shear loading. The second family uses rectangular boxes to apply complex loading to the specimen. In 1984, Peters [58] obtained an experimental curve of compression/shear buckling with a square section box stressed in torsion and bending. Klein [59] used a box structure embedded at one end and loaded with two actuators at the other end. Very recently, Zucco et al. [60] designed and manufactured a testing fixture capable of introducing a prescribed shear force and bending moment at one end of a variable thermoplastic composite wingbox and reacting the load at the other end. This test rig is self-equilibrated and so does not need any joints with the ground (foundations).

Castanié et al. [52, 61] developed a multiaxial test rig for asymmetric sandwiches with a box structure. The specimen is bolted to the test rig center on its upper face. Specimen overall dimensions are $248 \times 306 \text{ mm}^2$ and the area of interest is $200 \times 200 \text{ mm}^2$. The two actuators at the box extremities allow the structure to be loaded in four-point bending and the

specimen in traction or compression. The two actuators in the box center allow the structure to be loaded in torsion and the specimen in shear. This test rig was successfully used to show that asymmetric sandwich structures are extremely strong in compression [52]. However Castanié et al. pointed out some drawbacks. As for the other test rigs of this type, it is very difficult to estimate the stress flows directly entering in the specimen because of the numerous structural redundancies and the non-linear behavior of asymmetric sandwich structures. Then, the use of small specimens induces Saint-Venant effects, which perturb the strain field. This is why a new experimental test rig called the “VERTEX test rig” was developed [53, 62]. It is based on the same philosophy as used in Castanié’s test and is described in Figure 2. The specimen is now larger (Figure 3-a) and is bolted to the structure with 128 fasteners, 8 and 10 mm in diameter (Figure 3-b). The VERTEX test rig was used in the present study to carry out complex loading tests.

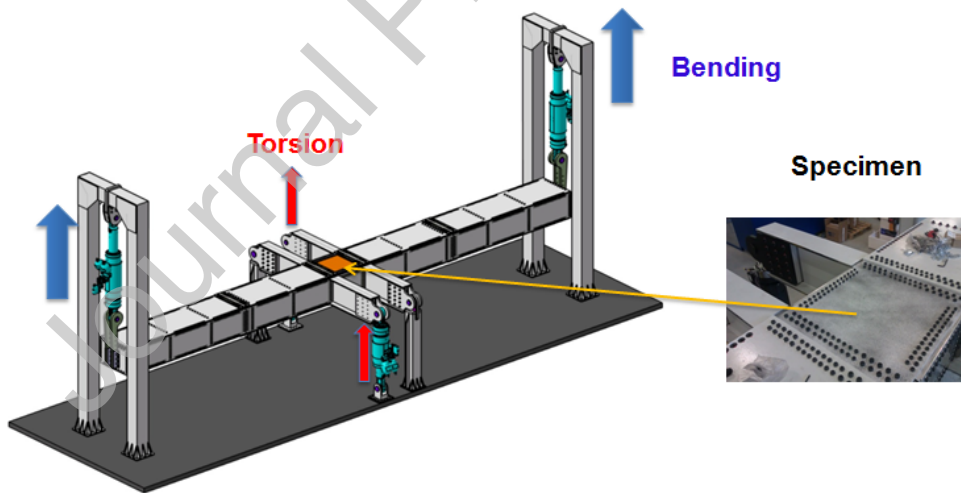
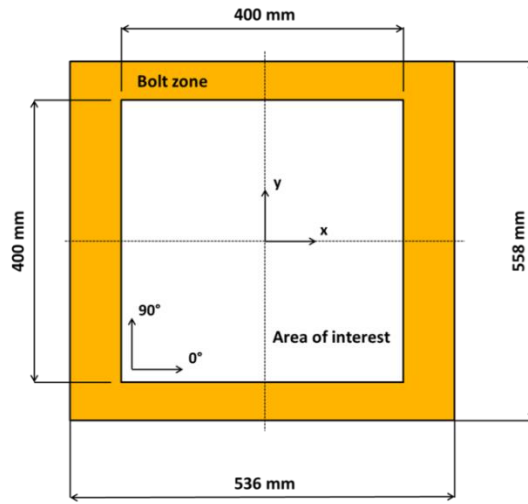


Figure 2: VERTEX test rig



(a)



(b)

Figure 3: (a) VERTEX specimen dimensions (b) VERTEX bolt zone

Testing specimens at the structural detail scale under combined loading is more complex than performing standard tests but detects mechanical phenomena that are much closer to those found in real-life structures. Standards recommended by industrials for low velocity impacts [7] and for compression after impact [8] on composite coupons are too conservative. For example, boundary conditions of the compression after impact standard impose a pure compression failure without postbuckling and the specimen size results in rapid propagation of the impact damage to the free edges. In real life, impacted panels are subject to postbuckling and it is interesting to study interactions between impact damage and postbuckling.

1.3. Objectives

The Discrete Ply Model (DPM) developed at the Institut Clément Ader by Bouvet et al. makes it possible to simulate low velocity impact and compression after impact, capturing matrix cracking, fiber breakage and delamination [2, 39, 63]. The DPM was validated for different stacking sequences with an experiment/model dialog in terms of delamination areas and force displacement curves. It has also shown good results with residual compression strength [39, 63] and has been used to optimize a composite laminate design according to low velocity impact damage tolerance [2]. More recently, simulation of notched behavior in tension has also been achieved with several scales of specimen [64-65].

In the present work, the DPM is used in a “Virtual Testing” approach to simulate medium velocity impacts (50 – 110 m/s) and complex loading after impact on large composite laminate plates. This medium speed range was chosen to simulate a new application case with the DPM. To adopt an original position, the laminate scale was chosen at the second level of the pyramid of tests [14]. As presented in the experimental part associated with this research [51], impacted plates were loaded under complex stresses in order to go further than the recommended standards [8], which seem conservative, and to be able to study interactions between impact damage and postbuckling. The complex loading after impact was obtained with the VERTEX test rig at the Institut Clément Ader [66]. The context of testing composite panels under complex loading with structural test rigs is discussed in detail by Castanié et al. in [52, 61] and the first tests achieved with the VERTEX test rig are presented in [53, 62].

A brief reminder is given of the DPM in Section 2, with a description of the numerical modeling used and the experimental campaign of impact and complex loading after impact.

Numerical and experimental results are compared: for medium velocity impact in terms of delaminated area and force displacement curves and for complex loading after impact in terms of loading paths. The aim is to validate the use of the DPM as a tool to study interactions between impact damage and postbuckling.

2. Numerical model and experimental campaign

The Discrete Ply Model “DPM” is extensively presented in [39, 63]. The DPM is run with Abaqus/Explicit and a VUMAT. The model is recalled only briefly here as further details have already been published [64]. In this section, damage modeling philosophy as well as the material and boundary conditions used, are described. Then the experimental campaign of impact and complex loading after impact is presented.

2.1. Discrete Ply Model

Figure 4 presents the concept of the DPM. The main failure modes occurring in an impacted composite laminate (matrix cracking, fiber failure and delamination) are taken into account in the model as follows:

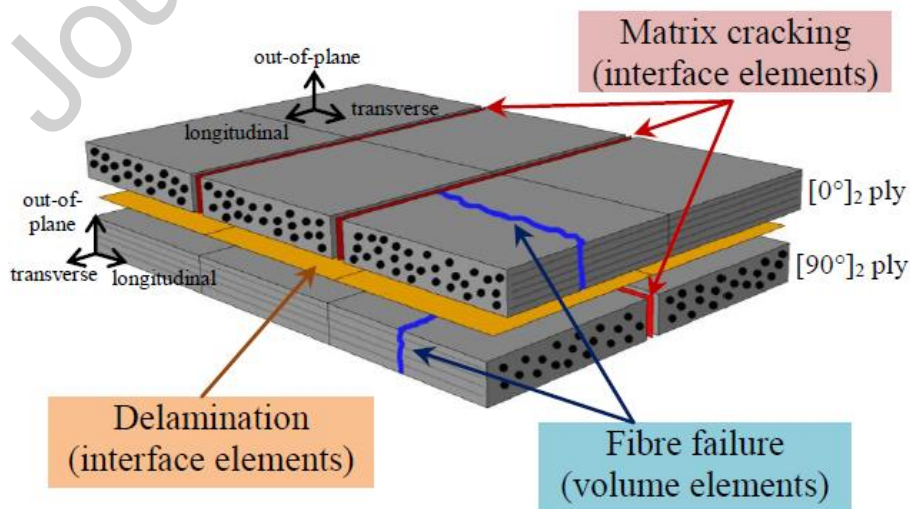


Figure 4: DPM concept: element types and associated damage [64]

- Delamination is simulated with classical interface elements between two consecutive plies, each ply being modeled with one 3D element in the thickness. This damage is driven using fracture mechanics. Once delamination is initiated, the propagation is modeled by releasing stresses until dissipation of the critical energy release rate.
- Matrix cracking is modeled with interface elements located between volume elements in the ply direction. This damage is driven using Hashin's Criterion (Eq. 1) calculated in neighboring volume elements.

$$\left(\frac{\sigma_t^+}{\sigma_t^f}\right)^2 + \frac{\tau_{lt}^2 + \tau_{tz}^2}{(\tau_{lt}^f)^2} \leq 1 \quad (\text{Eq. 1})$$

with σ_t^+ the positive value of the transverse stress, σ_t^f the transverse failure stress, τ_{lt} and τ_{tz} the shear stresses, and τ_{lt}^f the shear failure stress. When the criterion is reached, element stiffness is set to zero, and the two volume elements become independent. The use of interface elements in the ply thickness imposes a complex mesh but allows the coupling between intra- and inter-laminar damage to be obtained naturally.

- Fiber failure is taken into account using conventional continuum damage and failure mechanics. When the damage initiation strain ε_0^t in traction or ε_0^c in compression is reached, a damage variable corresponding to a linear decrease of the stress is calculated until the final damage strain ε^1 is obtained, and stresses are determined from the damaged stiffness matrix. ε^1 is calculated to ensure that the fiber critical energy release rate in mode I, $G_I^{f,t}$ in traction or $G_I^{f,c}$ in compression, is dissipated. The following equation (Eq. 1) describes the fiber failure criterion.

$$\int_V \left(\int_0^{\varepsilon_l} \sigma_l d\varepsilon_l \right) . dV \quad (\text{Eq. 2})$$

$$= S . G_l^f$$

where V and S are the volume and the section of the element and σ_l and ε_l the longitudinal stress and strain.

2.2. Material and boundary conditions

Medium velocity impact and complex loading after impact were performed on $558 \times 536 \times 3.5 \text{ mm}^3$ laminate plates of T700/M21 UD carbon/epoxy composite. The stacking sequence chosen for this model was quasi-isotropic, with 14 plies $[45_2/-45_2/0_2/90_2/0_2/-45_2/45_2]$. The ply thickness was 0.25 mm. Material properties used in the DPM are presented in Table 1. Figure 5 shows the mesh and numerical boundary conditions used in the model. In this figure, only half the plate is represented for better visualization.

Two zones were meshed with different elements. The central part ($270 \times 270 \text{ mm}^2$) was meshed with damageable C3D8 volume elements and different DPM damaging laws were taken into account. For this part, each ply was meshed with one volume element in the thickness and the element size was $1.64 \times 1.64 \times 0.5 \text{ mm}^3$. An intermediate zone was meshed with the same elements (one element per ply along the thickness) but without any damage behavior (elastic behavior only). The exterior part was meshed with non-damageable SC8R thick shell elements. Only one shell element was used in the specimen thickness and the element size was $5 \times 5 \times 3.5 \text{ mm}^3$. The stacking sequence of the specimen and its elastic properties (Table 1) are associated in these shell elements. The use of these elements allowed us to introduce exactly the same boundary conditions as were used with the implicit model [51] and to decrease computation time. These two different parts were tied with a node to surface constraint [67].

The specimen was impacted at its center by a 28 g hemispherical impactor 19 mm in diameter (Figure 5). The boundary conditions during the impact test were given by the contact between the plate and a fixed rigid body, representing the impact window ($400 \times 400 \text{ mm}^2$). After the impact step, a step of relaxation was simulated to eliminate vibrations and waves induced by the impact. During the step of loading after impact, displacements were imposed from DIC (Digital Image Correlation), as presented in a previous article [51], in order to recreate stress flows entering the specimen (Figure 5). The model was run with Abaqus/Explicit for each step. The step time was set to 30 ms, while the real test of loading after impact lasts about 3 min. Therefore, the DPM capability to simulate quasi-static tests is also assessed.

Table 1. T700/M21 properties used in the model

<i>Elastic Properties</i>		
E_l^t	<i>Tensile Young's modulus in fiber direction</i>	130 GPa
E_l^c	<i>Compressive Young's modulus in fiber direction</i>	100 GPa
E_t	<i>Transverse Young's modulus</i>	7.7 GPa
ν_{lt}	<i>Poisson ratio</i>	0.3
G_{lt}	<i>Shear modulus</i>	4.75 GPa
<i>Delamination & matrix cracking</i>		
σ_t^f	<i>Transverse tensile strength</i>	60 MPa
τ_{lt}^f	<i>In-plane shear strength</i>	110 MPa
G_{Ic}^d	<i>Interface fracture toughness for opening mode (I)</i>	0.5 N/mm
G_{IIc}^d	<i>Interface fracture toughness for shear mode (II & III)</i>	1.6 N/mm
<i>Fiber Failure</i>		
ε_0^T	<i>Fiber tensile strain at damage initiation</i>	1.70 %
ε_0^c	<i>Fiber compressive strain at damage initiation</i>	1.40 %
G_t^f	<i>Fiber tensile fracture toughness</i>	90 N/mm
G_c^f	<i>Fiber compression fracture toughness</i>	30 N/mm

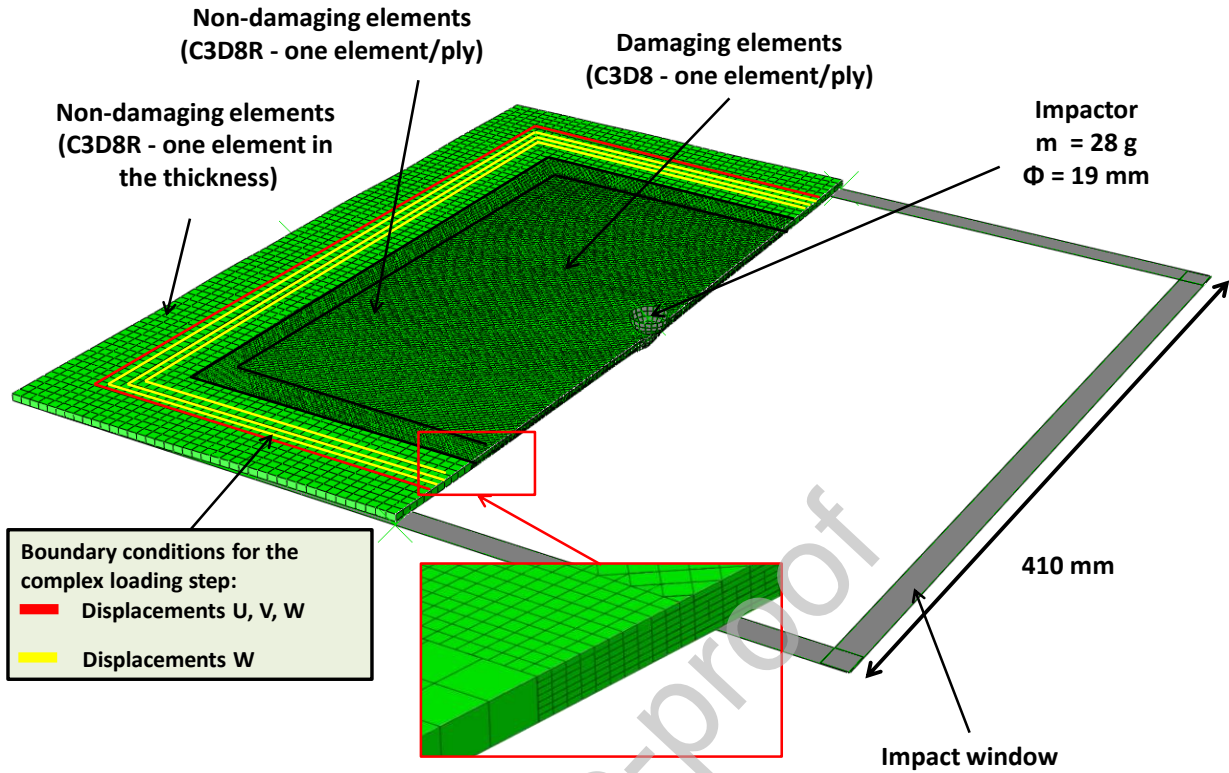


Figure 5: Boundary conditions of the finite element model

2.3. Experimental campaign

An experimental campaign was performed in order to validate the use of the DPM as a numerical tool, to predict damage occurring during medium velocity impact, and to evaluate the residual strength of the impacted structure under multiaxial loading. Eight specimens were draped. Seven of them (specimens A to G) were impacted at different medium velocities from 54 m/s to 110 m/s and one was kept non-impacted (specimen H). Impacts were performed with the gas launcher LG40 (a 40 mm diameter gas gun) of the impact platform STIMPACT [68]. After impact, all these specimens underwent different loading in the VERTEX test rig. During the impact phase, a speckled pattern was made on the impactor and its trajectory was tracked with a high-speed camera. Images recorded with the high

speed camera were processed with a program developed by Passieux et al. [69] to evaluate the impactor displacement and thus the impact force. The delaminated area after impact was evaluated with ultrasonic investigations. Curves of impact force versus impactor displacement and C-scan for each specimen are compared to numerical results (Figure 6 and Figure 7. For post-impact loading in the VERTEX test rig, a pair of 5 Mpx cameras recorded images from the speckled pattern made previously on the whole specimen. Then DIC software (VIC3D) was used to compute displacement and strain fields. Both the impact and post-impact test setups are presented in detail in the experimental part of this research [51]. The impact velocities and type of post-impact loading selected for each specimen are summarized in Table 2.

Table 2. Overview of impact velocities and post-impact loadings

<i>Specimen</i>	<i>Velocity (m/s)</i>	<i>Impact Energy (J)</i>	<i>Loading after impact</i>
<i>A</i>	<i>54</i>	<i>40.8</i>	<i>Compression/shear</i>
<i>B</i>	<i>70</i>	<i>68.6</i>	<i>Shear</i>
<i>C</i>	<i>75</i>	<i>78.7</i>	<i>Shear/tension</i>
<i>D</i>	<i>90</i>	<i>113.4</i>	<i>Compression/shear</i>
<i>E</i>	<i>98</i>	<i>134.4</i>	<i>Compression</i>
<i>F</i>	<i>100</i>	<i>140</i>	<i>Shear/tension</i>
<i>G</i>	<i>110</i>	<i>169.4</i>	<i>Compression</i>
<i>H</i>	<i>0</i>	<i>0</i>	<i>Shear/tension</i>

3. Validation of the numerical predictions

3.1. Impact

Experimental and numerical results in terms of delaminated area and curves of impact force versus impactor displacement are shown in Figure 6 (specimens A to C) and Figure 7 (specimens D to G). Concerning the delaminated area, except for specimen A, the extension of the delamination area at 45° at the lower interface is well propagated with the DPM. For other interfaces, the numerical delaminated area is a little greater than the experimental one. This explains why the global delaminated area, except for specimen A, is slightly overestimated even though the correlation between experimental and numerical results remains efficient. Experimental and numerical curves of impact force versus impactor displacement are also similar, except for specimen A, where the numerical impactor displacement is underestimated. This small value of displacement can explain the poor numerical delamination obtained at the lower interface for specimen A. In fact, the delamination propagation at the lower interface is due to the overall bending of the structure. These results demonstrate the capabilities of the DPM to simulate a medium velocity impact on a large composite plate.

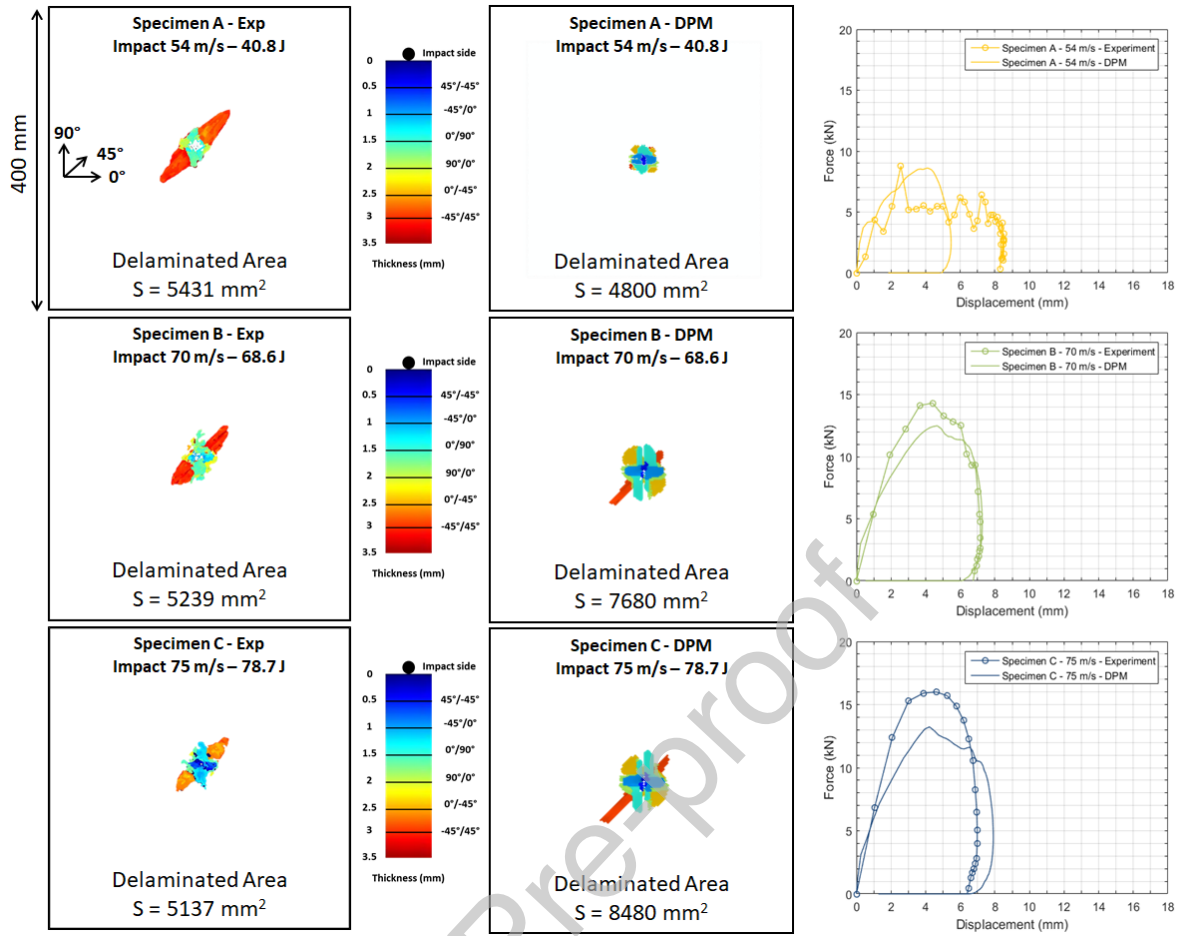


Figure 6: Delaminated areas and curves of impact force versus impactor displacement for impact energy less than 100 J. Left column: Experimental, Middle: DPM, Right: force - displacement curves Exp vs DPM

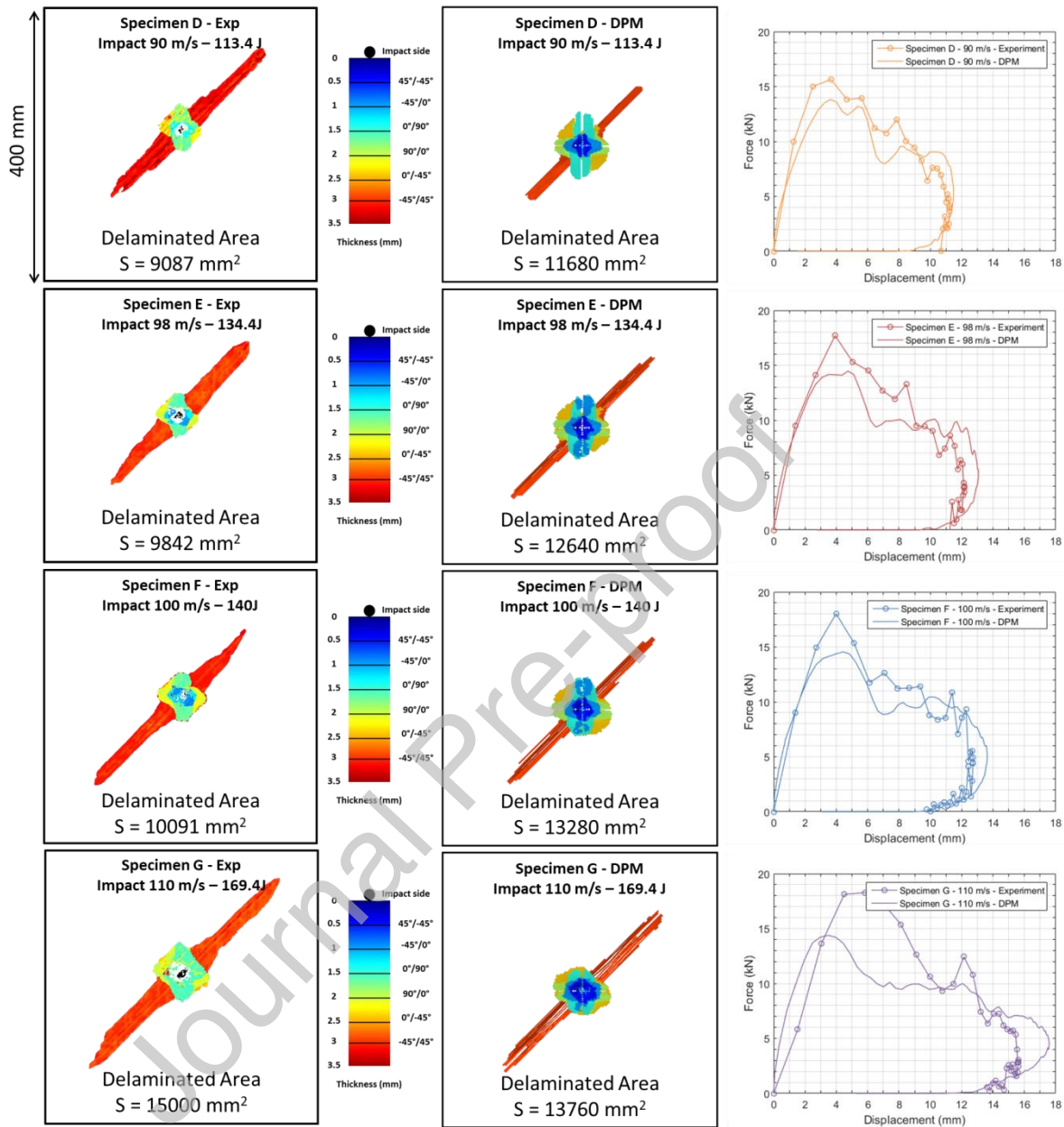


Figure 7: Delaminated area and curves of impact force versus impactor displacement for an impact energy higher than 100 J. Left column: Experimental, Middle: DPM, Right: force -displacement curves Exp vs DPM

3.2. Complex loading after impact

In this work, the numerical and experimental results of combined loading after impact were compared for specimens A, B, C, F and G. Therefore, every type of loading was simulated: compression, shear, compression+shear and tension+shear. The pure tension case was not tested because the tension flux needed to break the impacted plate would have been too close to the limits of the VERTEX multiaxial rig (3000 N/mm). Boundary conditions were applied as displacement on the top surface, as described in Figure 5. For each case, numerical stress/strain curves obtained with the DPM (with and without the simulation of the impact) were compared to stress/strain curves obtained with the experiment. DPM stress/strain curves were obtained with the same method as the experimental curves, as presented in detail in [51]. The methodology to determine average stresses and global strains from displacement obtained with the help of stereo digital image correlation is briefly recalled in Figure 8. A comparison between numerical and experimental results, in terms of fiber failure scenario, delamination area evolution and displacements was also performed.

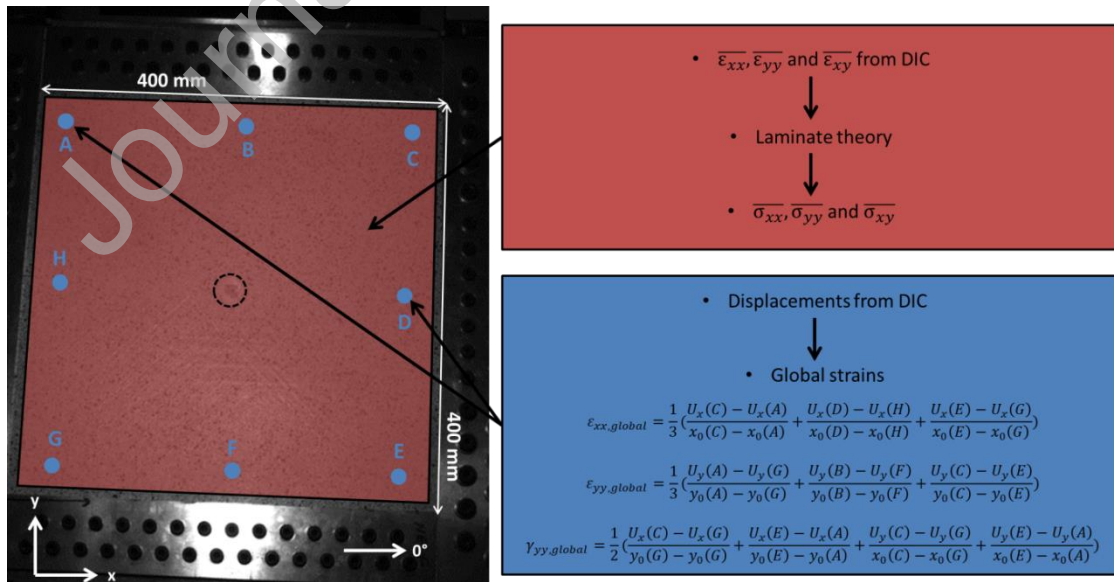


Figure 8: Method to determine average stresses and global strains [51]

Compression/shear test (specimen A)

Specimen A, impacted at 54 m/s, was loaded in compression/shear. Stress/strain curves are shown in Figure 9. In compression/shear, curves follow the theoretical and experimental stiffness until the buckling appears. Numerical failure appears earlier than the experimental one when the shear behavior is examined. No difference is visible whether the impact is simulated or not. This is consistent with the very small delaminated areas obtained after impact (numerically and experimentally).

The DPM simulation makes it possible to analyze the failure scenario. The fiber failure is initiated in the bottom right corner and propagated through the impact point to reach the opposite corner (Figure 10). This is very consistent with thermal images recorded during the real test [51], which show that heat was first emitted in the bottom right corner. The upper ply is oriented at 45°. It was loaded in compression during impact and loaded again in compression during shear loading. It is therefore not surprising to observe it failing first in compression fiber failure mode.

The DPM shows that the delaminated area after impact is still the same as when the first failure occurred and does not evolve during the failure propagation (Figure 11). Only a delamination propagation according to fiber failures in the top ply appears.

Figure 12 compares displacement fields between experimental results and numerical results just before total failure of the specimen. The fields of displacement shapes are very well described.

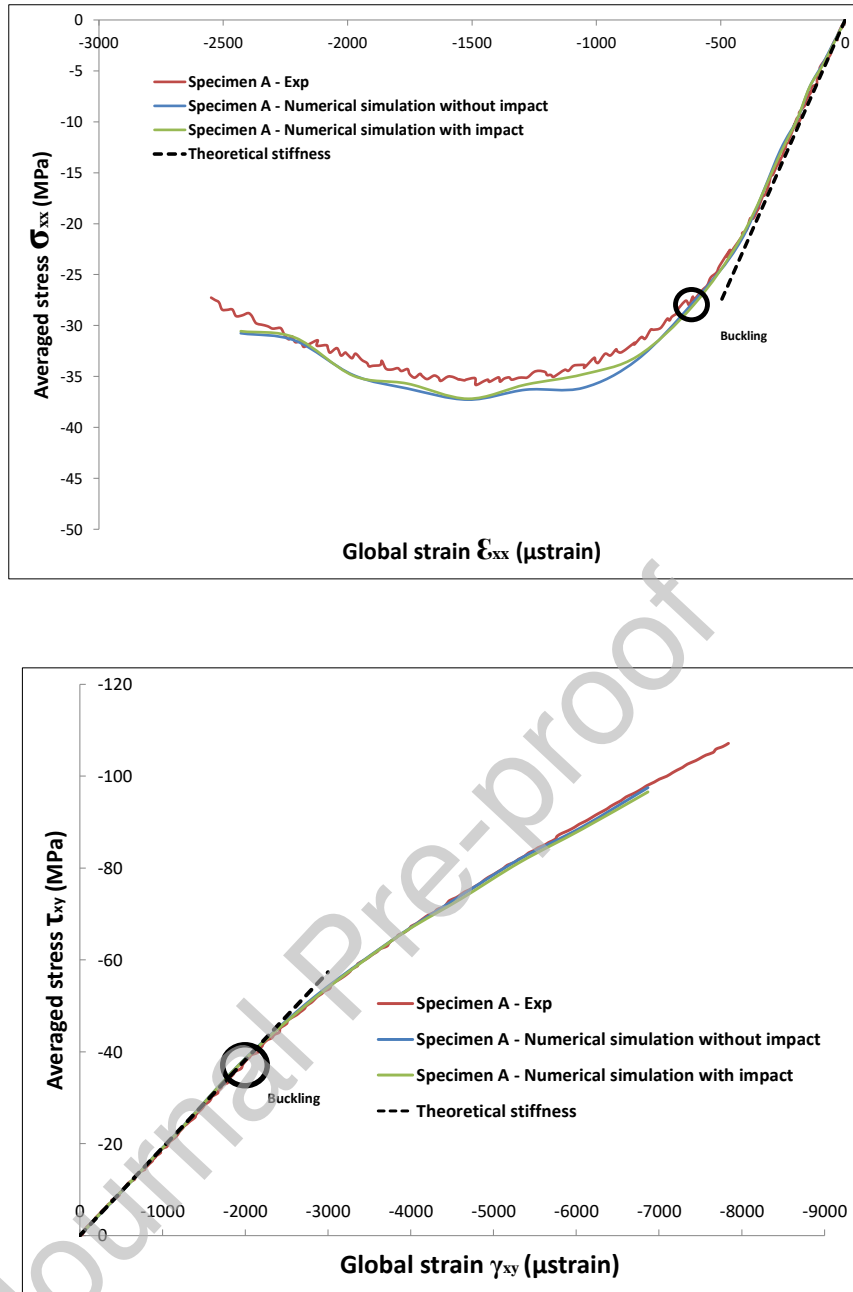


Figure 9: Stress/Strain curves for specimen A in Compression/Shear loading

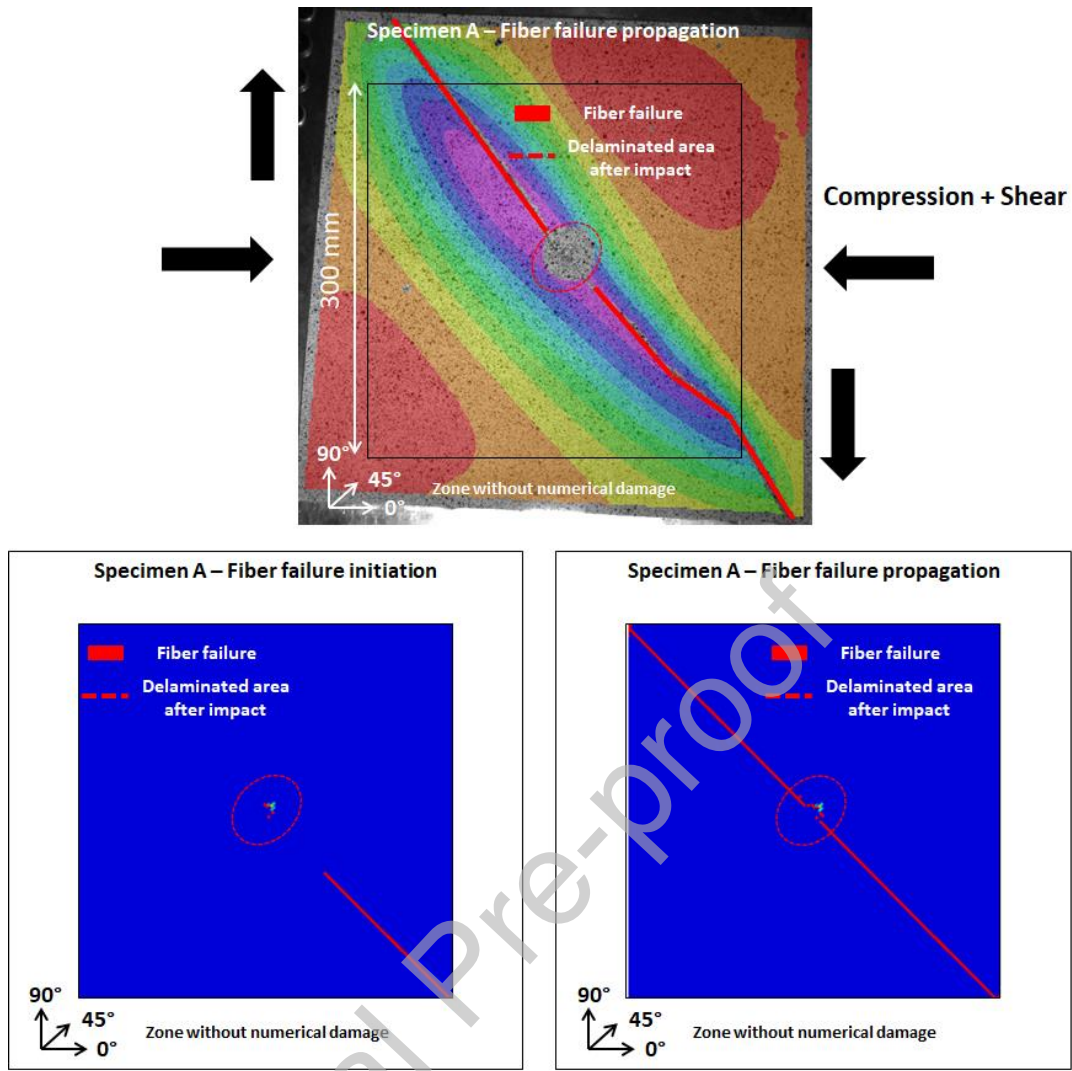


Figure 10: Comparison between DPM and experimental failure profile for specimen A

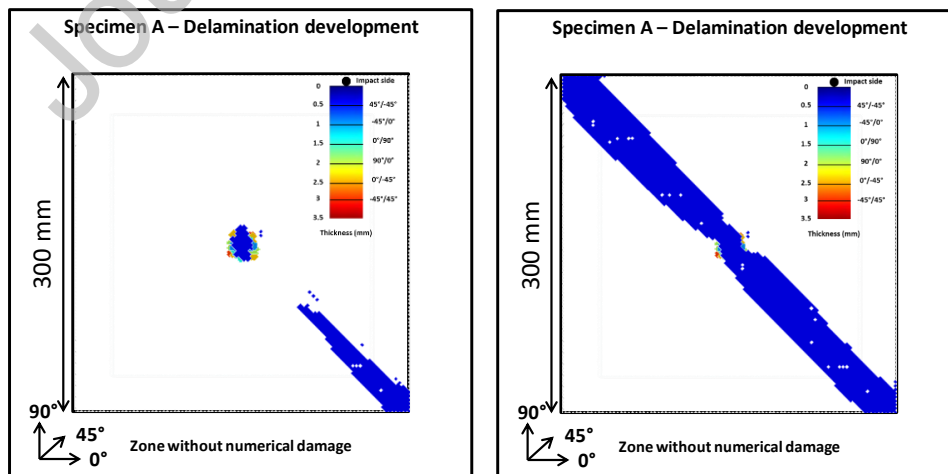


Figure 11: Delamination evolution during the loading after impact for specimen A

Compression/shear (specimen A)

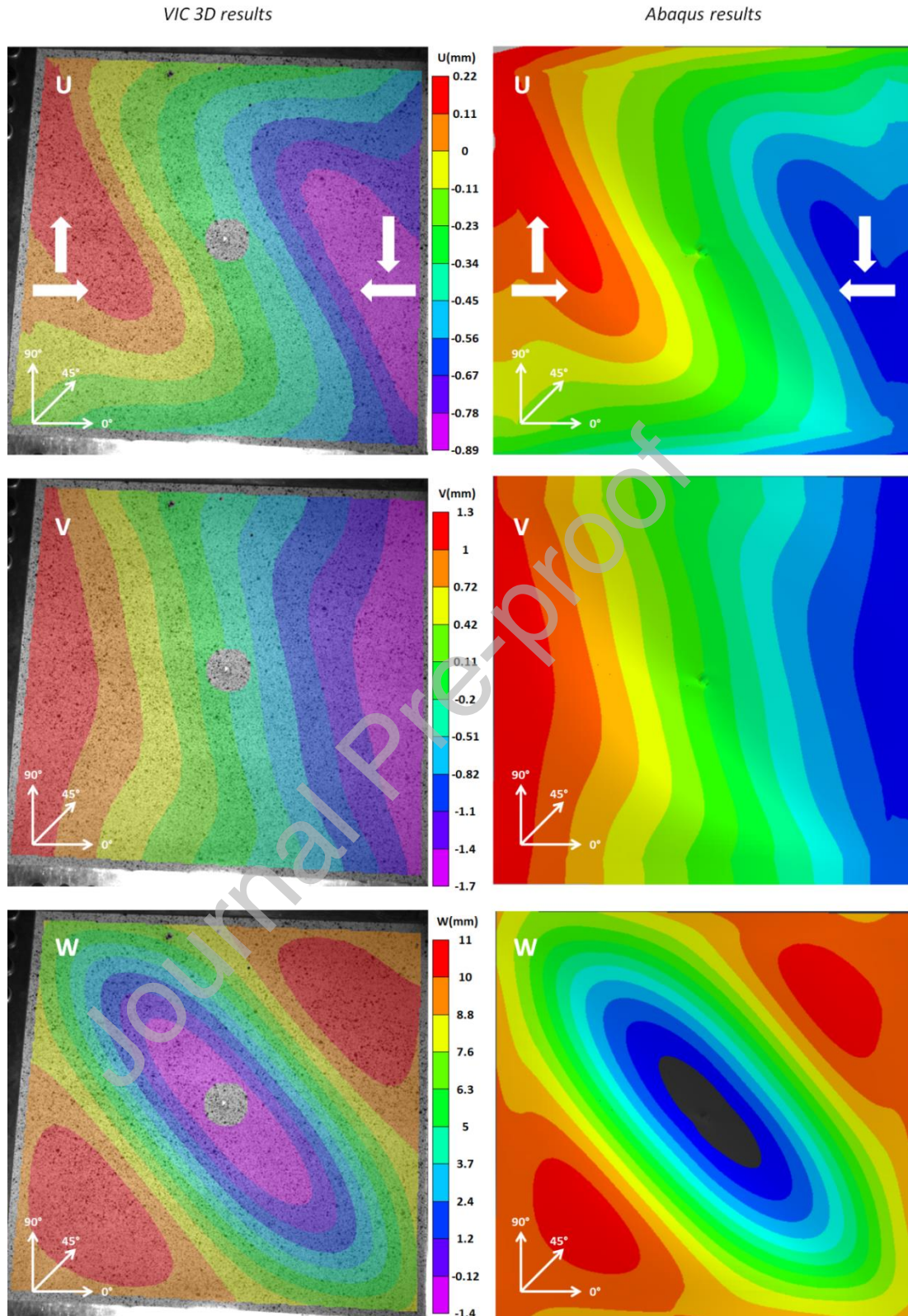


Figure 12: Experimental and DPM displacement fields in compression/shear just before failure

Shear test (specimen B)

Specimen B (impacted at 70 m/s) was loaded in shear. The stress/strain curves corresponding to this test are plotted in Figure 13. The normal stress (σ_{xx}) is not displayed since it was very close to a horizontal line. The curves obtained with the DPM follow the experimental and theoretical stiffness until buckling appears. Afterwards, numerical and experimental behaviors are similar until partial failure appears for the experiment. This failure is not well reproduced by the models and therefore the numerical failure stress is higher than expected. As for specimen A, no difference is visible whether the impact is simulated or not. This is consistent with the very small delaminated areas obtained after impact (numerically and experimentally).

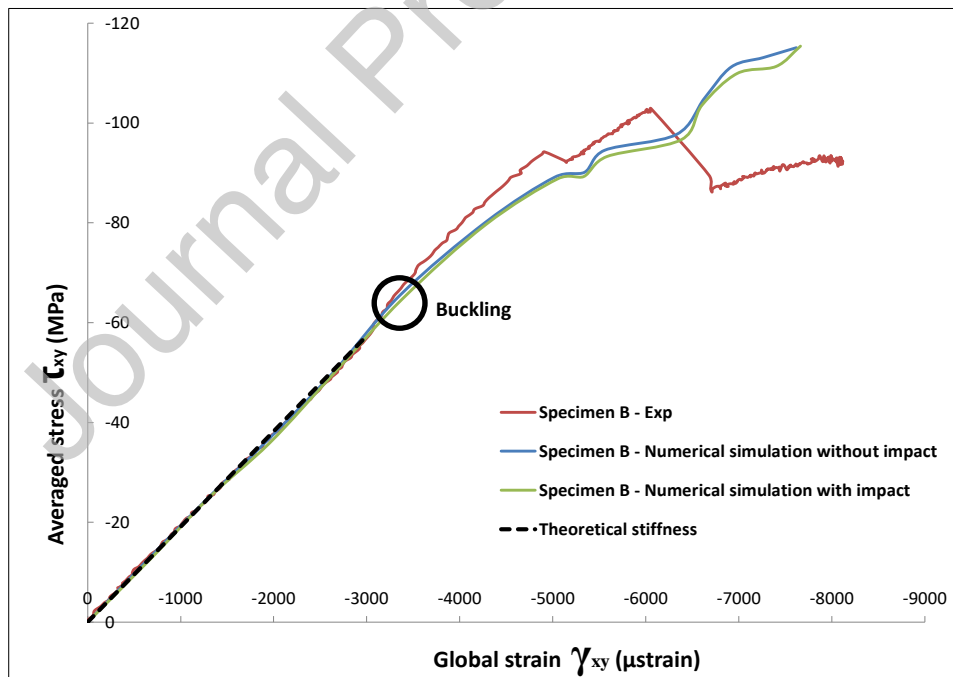


Figure 13: Stress/strain curves for specimen B in shear loading

Concerning the failure profile (Figure 14) with the DPM simulation, the failure is initiated in the bottom right corner and propagated through the impact point to reach the opposite corner. This is in contradiction with images recorded during the real test, which seem to show that failure is initiated in the impact zone, and then propagates to the bottom right and the top left corners. This may be explained by a poor quality of the boundary conditions associated with a poor displacement correlation due to several specular reflections of light on the speckle pattern (Figure 16). The discrepancy may also stem from an insufficient simulated fiber failure on the impacted side, since this probably initiates the global failure.

The DPM shows that the delaminated area after impact is still the same as when the first failure occurred and does not evolve during the failure propagation (Figure 15). Only a delamination propagation according to fiber failures in the top ply appears. Figure 16 compares displacement fields between experimental results and numerical results. The displacement fields are correctly described but the amplitudes are slightly overestimated (grey and black zones). In other words, the post-buckling behavior is overestimated. This corroborates the observations made on Figure 13.

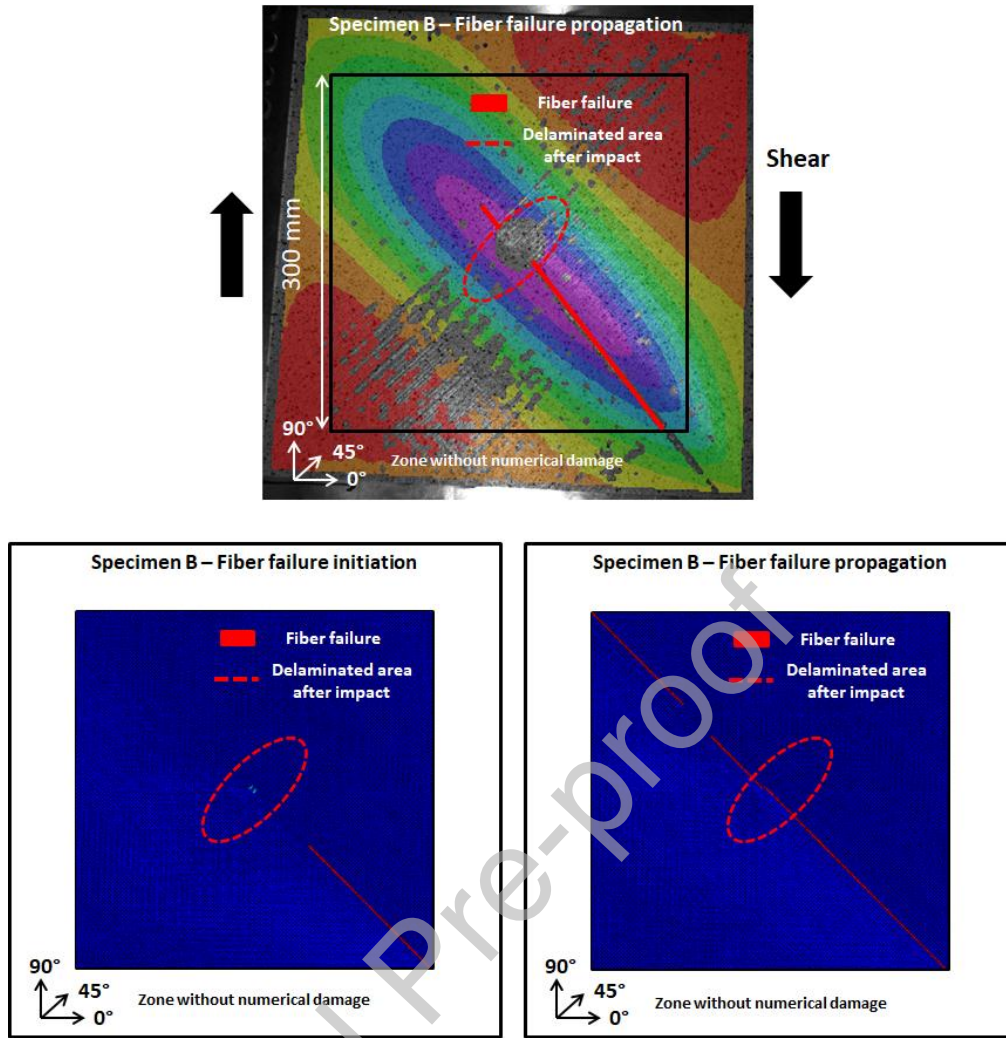


Figure 14: Comparison between DPM and experimental failure profile for specimen B

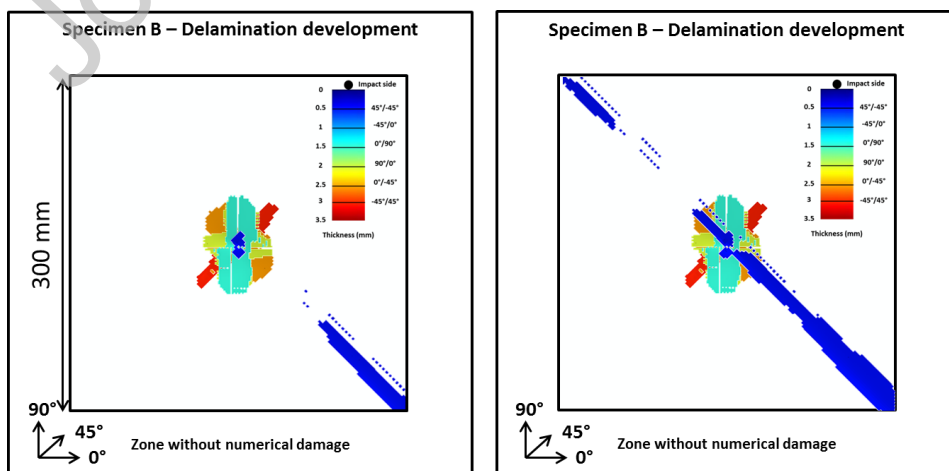


Figure 15: Delamination evolution during the loading after impact for specimen B

Shear (specimen B)

VIC 3D results

DPM results

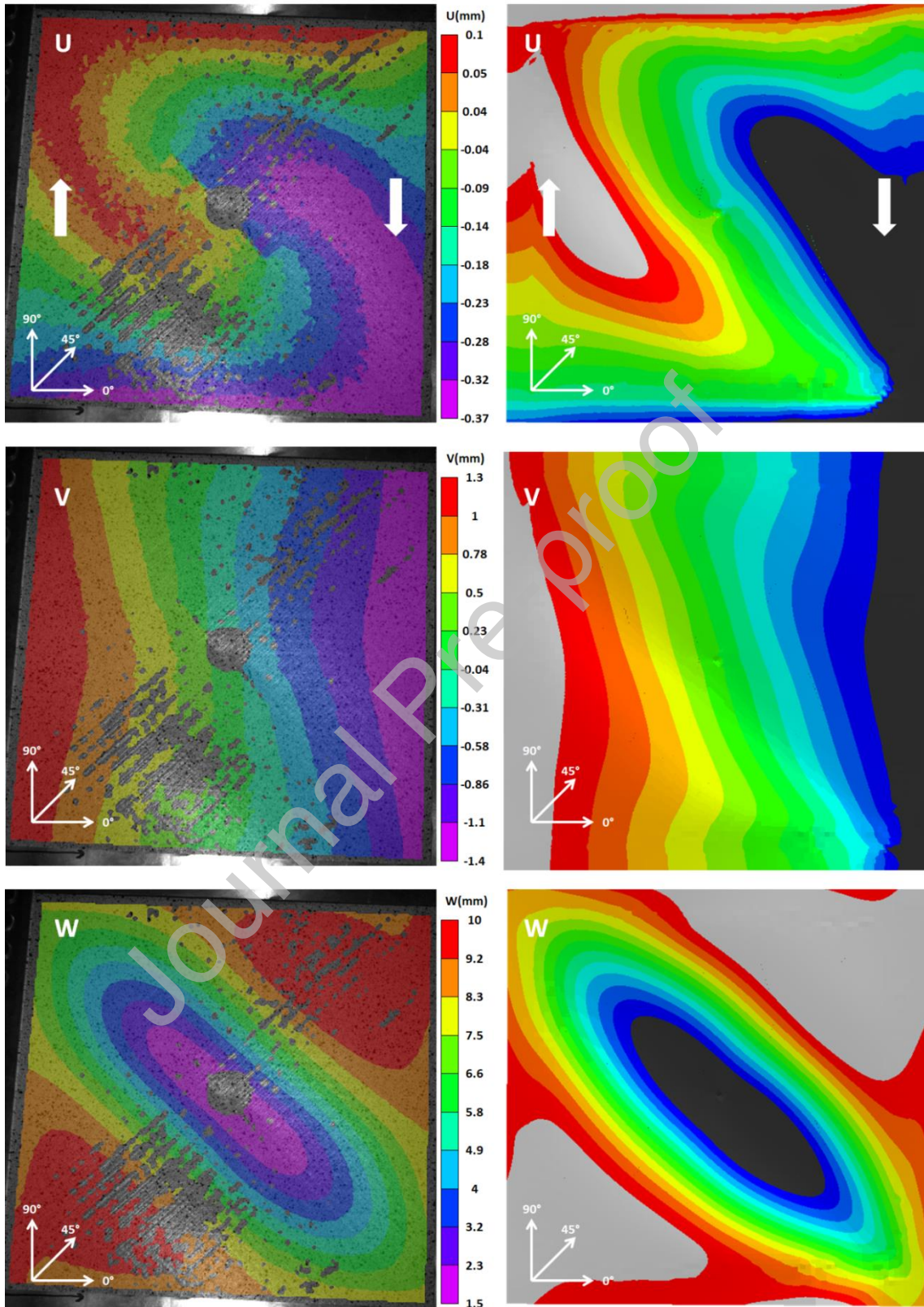


Figure 16: Experimental and DPM displacement fields in shear just before failure

Tension/shear test (specimen C)

Specimen C (impacted at 75 m/s) was subjected to tension/shear loading. The stress/strain curves (Figure 17) allow the tensile and shear behaviors to be analyzed. In tension and in shear, the numerical stiffnesses are very similar to both the theoretical and the experimental values until the buckling point is reached. The correlation of the buckling point is very good for the shear behavior but there is a small difference in the tension behavior: the buckling point is underestimated. After the buckling, the global strain value decreases as the experimental value and the stress continues to increase. The final failure occurs around the same stress value but the numerical failure longitudinal strain ($-500 \mu\text{def}$) is notably lower than the real failure strain ($-200 \mu\text{def}$). This difference is due to underestimation of the buckling point by the numerical models: the curves are shifted to the left of the figure but follow the same trend. Of course, this discrepancy should be considered with caution, given the very low value of the imposed longitudinal strain. In shear after buckling, the behavior is well simulated by the numerical models. Simulating the impact does not have a substantial influence here; only the final failure appears earlier (tensile behavior) when it is taken into account.

The DPM final failure profile (Figure 18) is close to the experimental failure. The numerical failure starts from the initial delaminated area due to impact and then propagates to both the top left and bottom right corners. The experimental data do not make it possible to confirm this scenario precisely because the damage propagates very suddenly. The infrared camera was not used at a high enough frame rate to capture its propagation in both directions. As for specimen B (in pure shear), the delaminated area after impact is not modified by the tension/shear loading (Figure 19). Only delamination according to the fiber failure in the top ply propagates. Figure 20 shows adequate correlation between DPM and

experimental displacement fields before failure. The displacement fields are correctly described but the amplitudes are slightly overestimated (grey and black zones). In other words, the post-buckling behavior is overestimated. This corroborates the observations made on Figure 17.

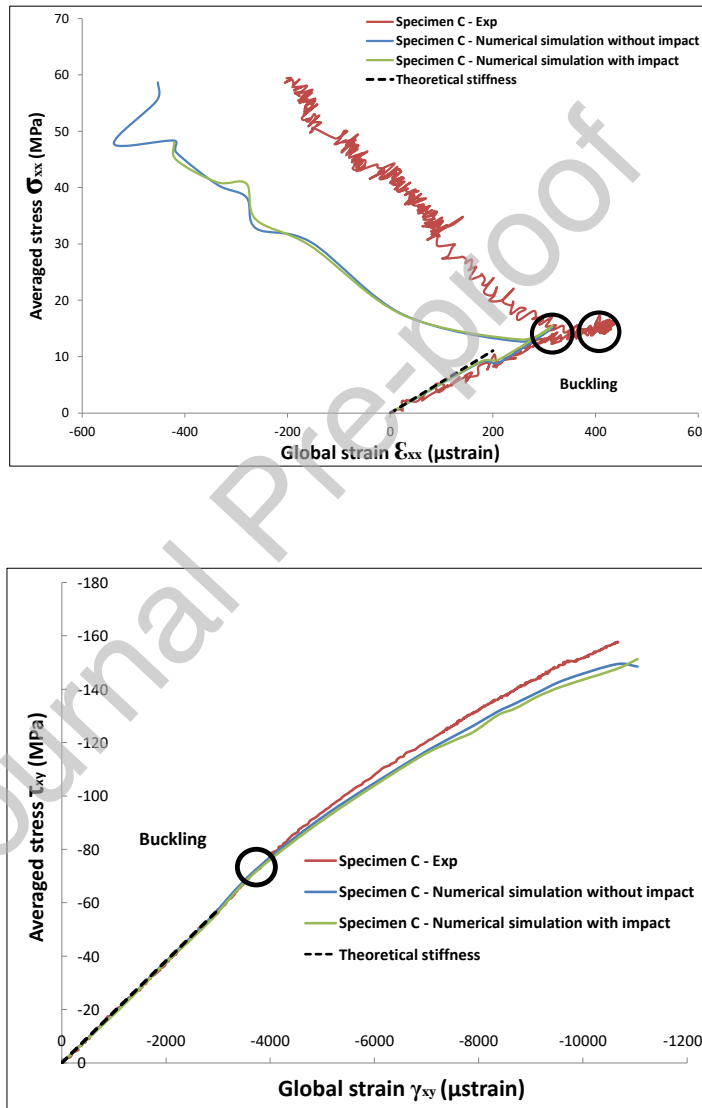


Figure 17: Stress/strain curves for specimen C in tension/shear loading

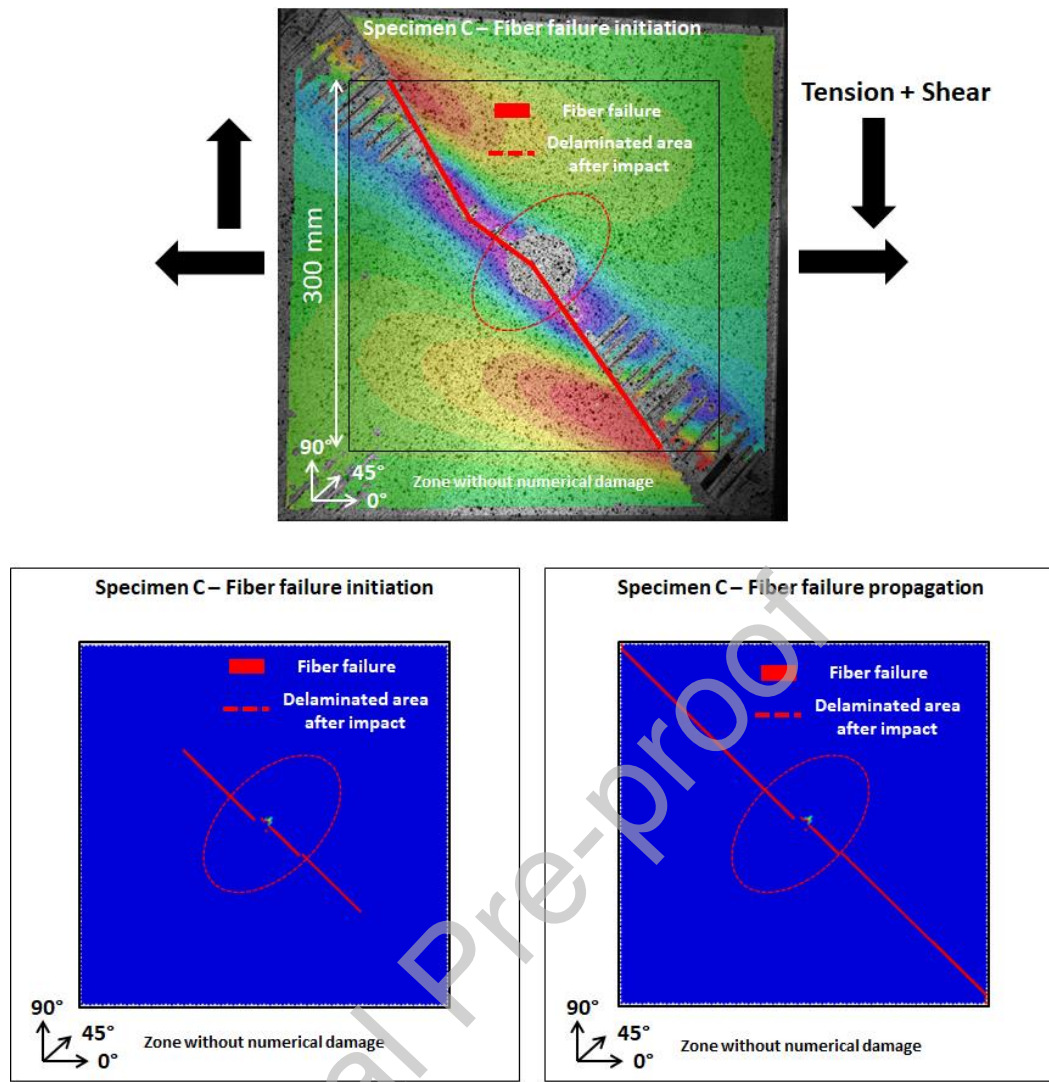


Figure 18: Comparison between DPM and experimental failure profiles for specimen C

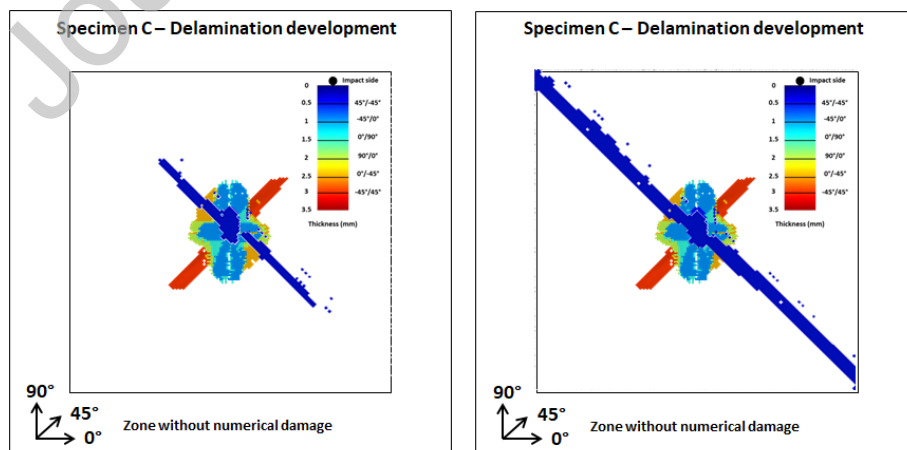


Figure 19: Delamination evolution during the loading after impact for specimen C

Tension/shear (specimen C)

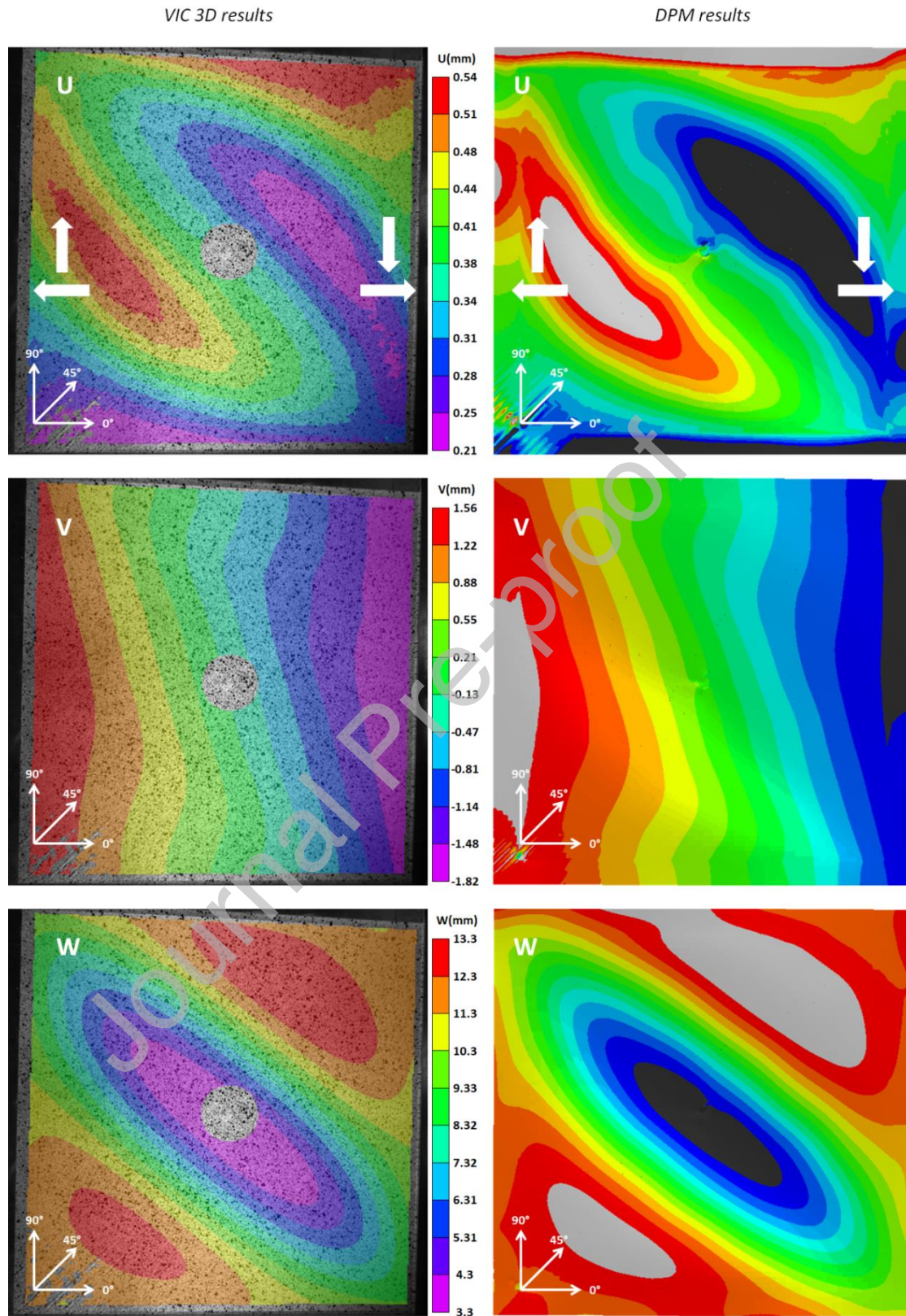


Figure 20: Experimental and DPM displacement fields in tension/shear just before failure

Tension/shear test (specimen F)

Specimen F, impacted at 100 m/s, was loaded in tension/shear. Stress/strain curves in tension and shear are shown in Figure 21. The oscillations observed on the experimental curves are simply due to the use of a higher number of data points during the testing of specimen F, which exhibit the servo-control of the multiaxial test-rig. In tension, curves follow the theoretical and experimental stiffness until the buckling appears. Numerically determined failure stress is lower than that found by experiment. Regarding the shear behavior, the initial stiffness is slightly overestimated by the simulations. The buckling point, and therefore the failure stress, is markedly underestimated by the numerical models. The behavior in tension for this specimen is better than for specimen C, which was also loaded in tension/shear but impacted at 75 m/s. The opposite is, however, true for the behavior in shear. No difference is detected whether the impact is simulated or not.

The numerical final failure profile is similar to the experimental failure profile. The fiber failure initiates in the bottom right corner (Figure 22) as observations made with the thermal camera in [51] suggested. Afterwards, fiber failure occurs in the top left corner and later in the central damaged area due to preliminary impact. Eventually, fiber failures coalesce in a global -45° orientated line. As for specimen C, also loaded in tension/shear, the failure scenario of specimen F is influenced by the initial damage. As for specimens A, B and C, the delaminated area after impact follows the fiber failure scenario exactly (Figure 23).

In Figure 24, DPM numerical and experimental displacement fields are compared. Numerically obtained displacements are comparable to those extracted from the experiment. The specular reflections due to a poor choice of paint for the speckle pattern (glossy instead of mat) led to zones of the images where the correlation was impossible to

estimate (bottom left corner). Therefore, incomplete displacement data led to incomplete boundary conditions and wrong simulations of the displacement in this area.

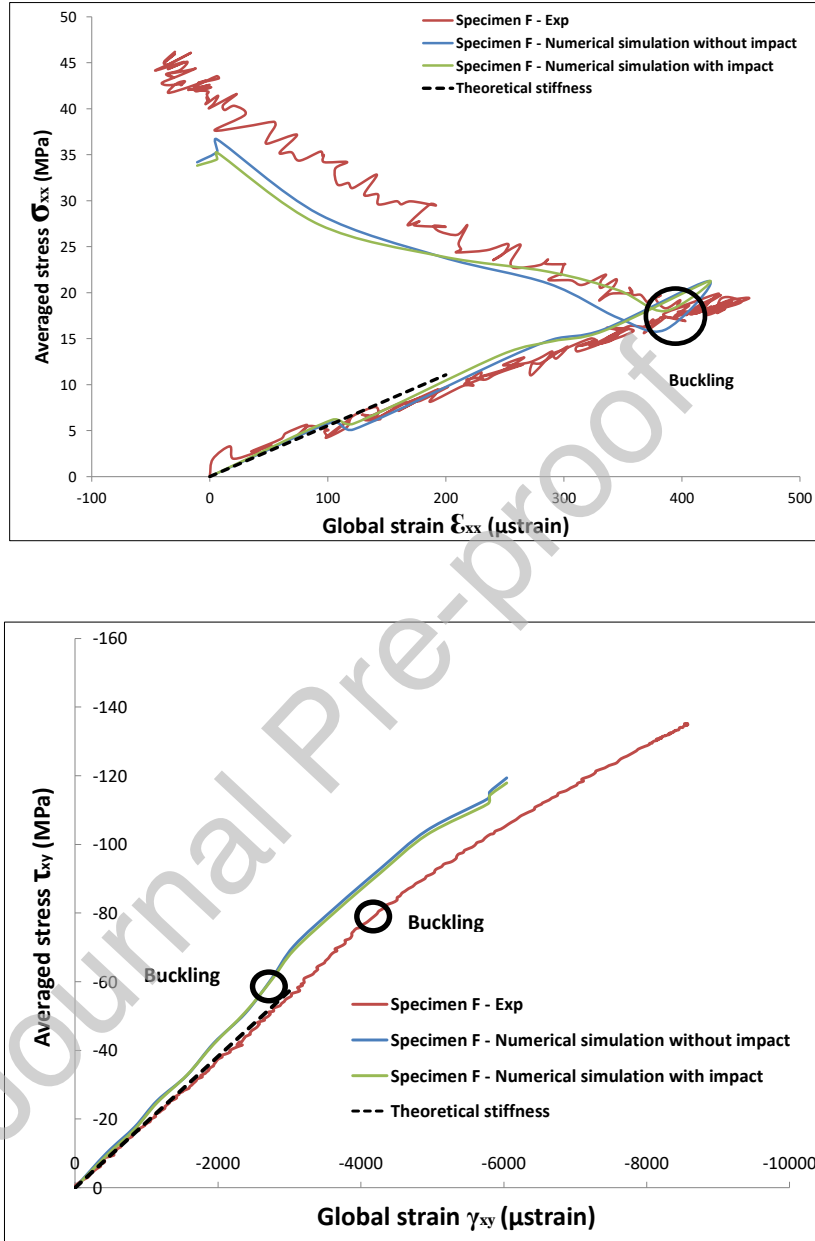


Figure 21: Stress/strain curves for specimen F in tension/shear loading

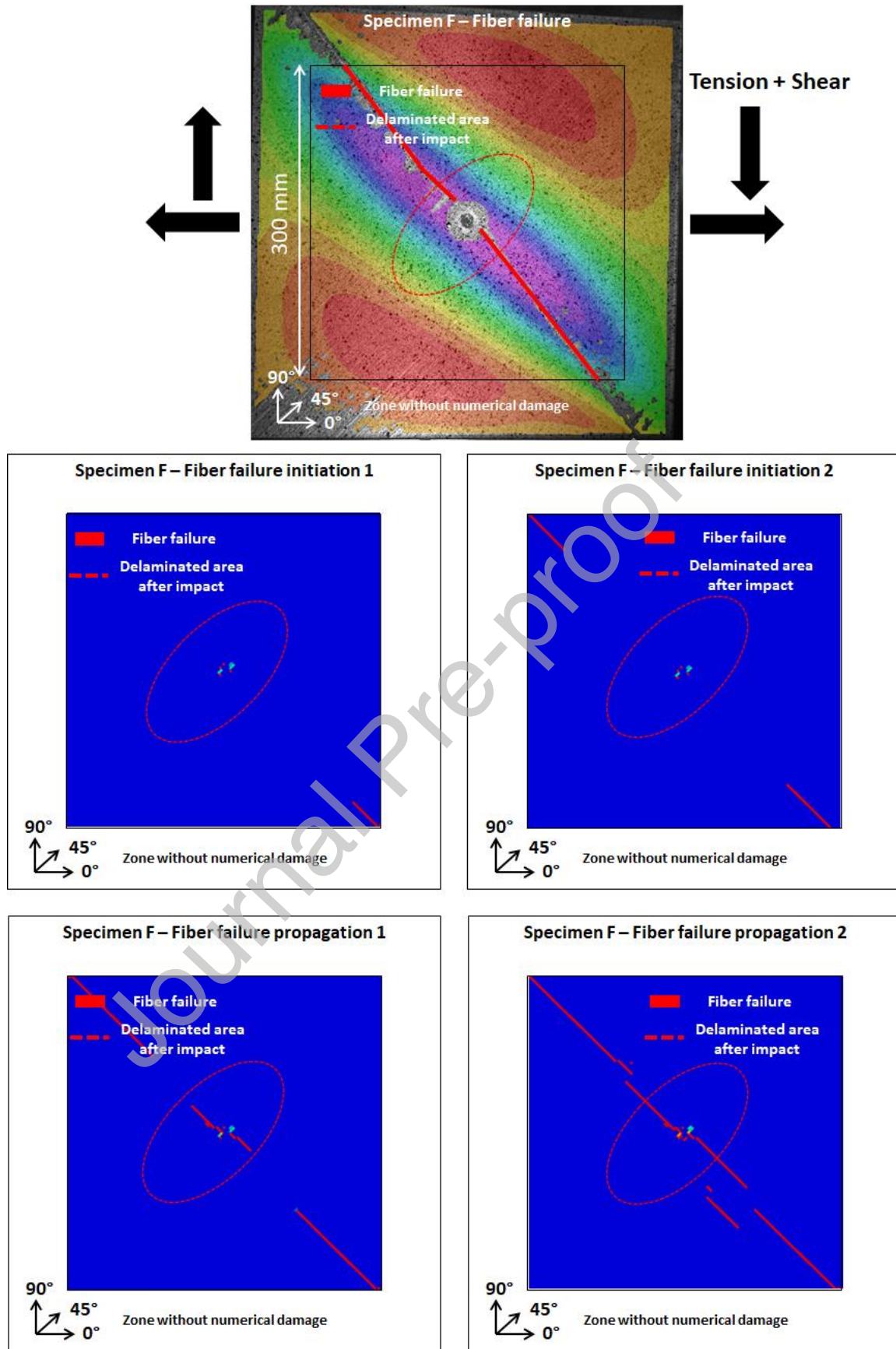


Figure 22: Comparison between DPM and experimental failure profile for specimen F

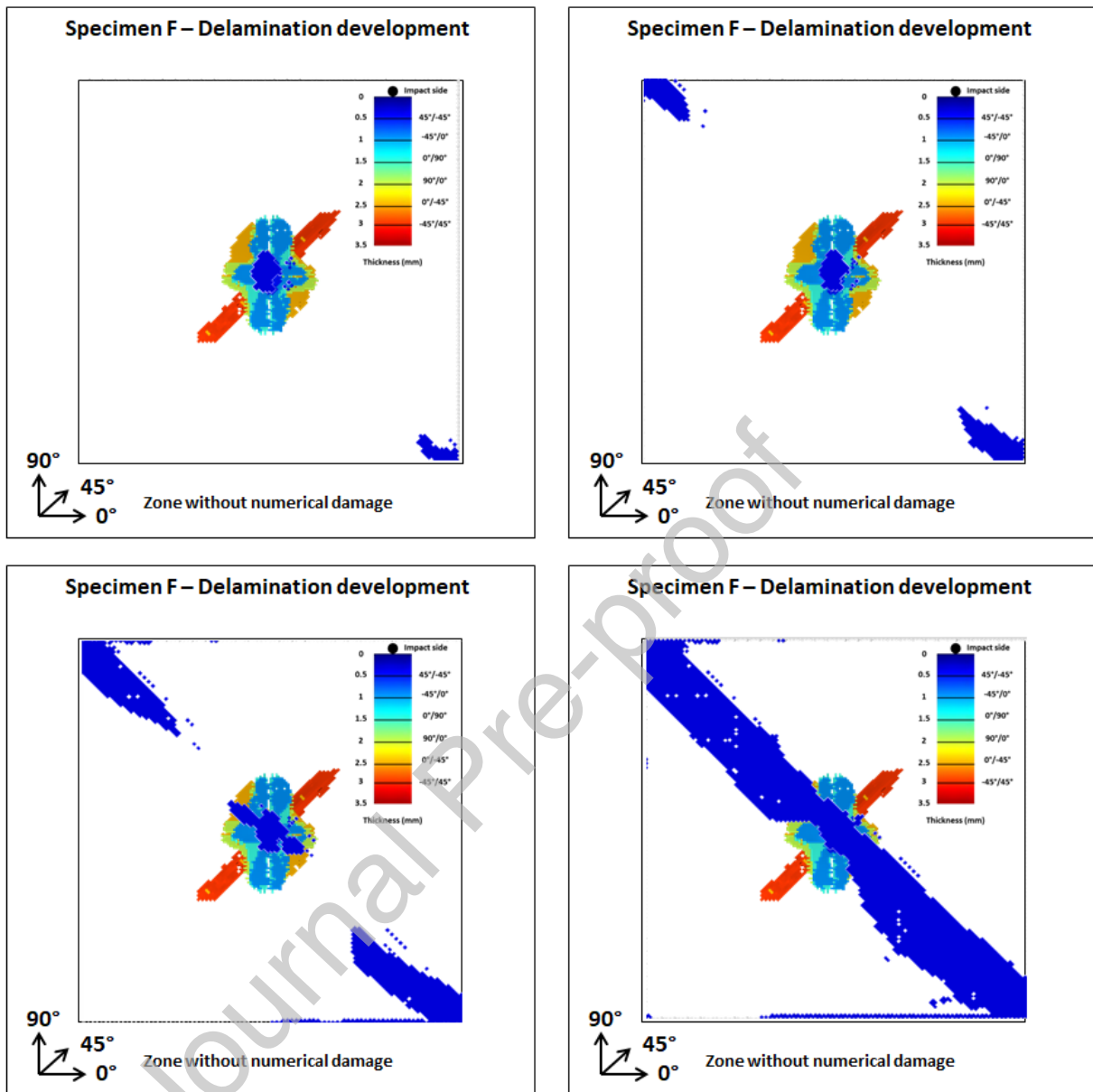


Figure 23: Delamination evolution during the loading after impact for specimen F

Tension/shear (specimen F)

VIC 3D results

DPM results

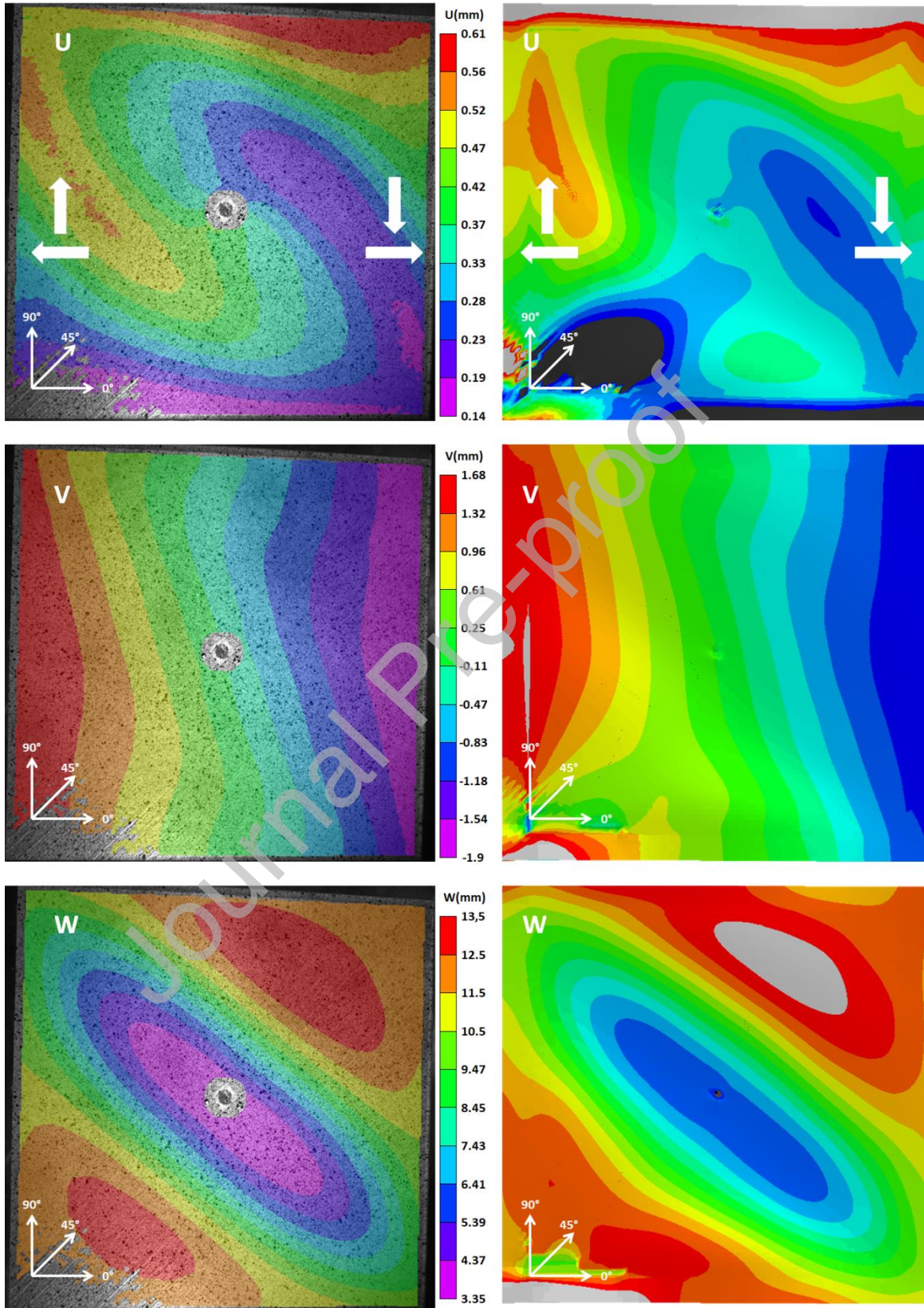


Figure 24: Experimental and DPM displacement fields in tension/shear just before failure

Compression test (specimen G)

Specimen G, impacted at 110 m/s, was loaded in compression and the corresponding stress/strain curves are shown in Figure 25. The curves follow the theoretical and experimental stiffness until buckling appears. The first and second buckling modes are correctly predicted by the models (Figure 25). After the second buckling, the numerically obtained behavior diverges slightly from the experimental one. This might have to do with the complex evolutions of the displacement fields due to two buckling modes and the way averaged stresses are obtained [51]. A small difference in the buckling behavior can translate into large difference in the averaged stress. No difference is seen whether the impact is simulated or not.

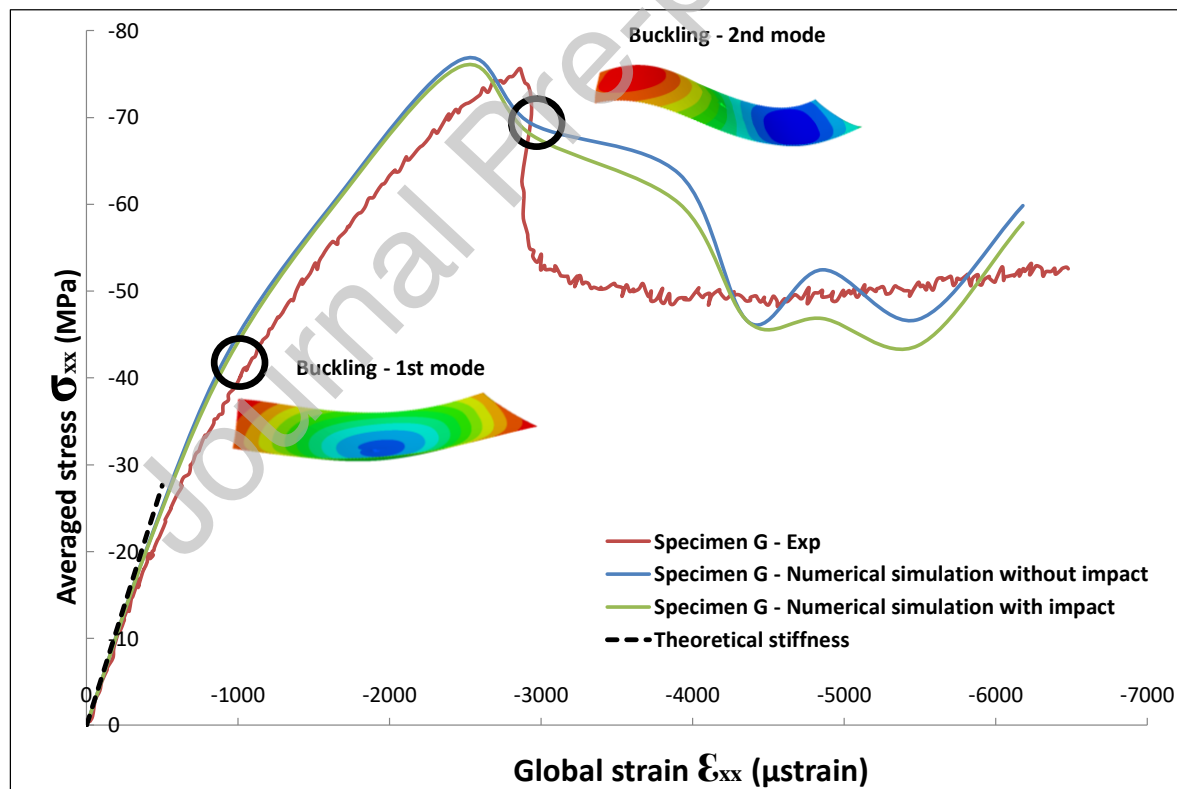


Figure 25: Stress/Strain curves for specimen G in Compression loading

Concerning the failure profile (Figure 26), the DPM simulation is consistent with the experiment since the failure is initiated in the bottom right corner and propagates towards the center of the plate. The numerically determined orientation is, however, different from that observed experimentally.

The DPM shows that the delaminated area after impact is still the same as when the first failure occurred and does not evolve during the failure propagation (Figure 27). Only a delamination propagation according to fiber failures in the top ply appears. A comparison of displacement fields between experimental and numerical results is shown in Figure 28. The displacement fields are correctly described.

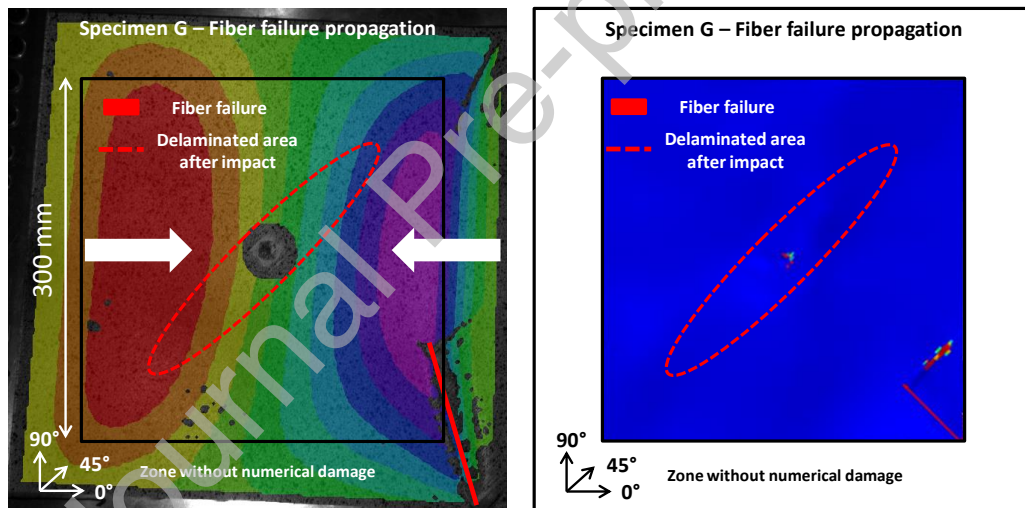


Figure 26: Comparison between DPM and experimental failure profile for specimen G

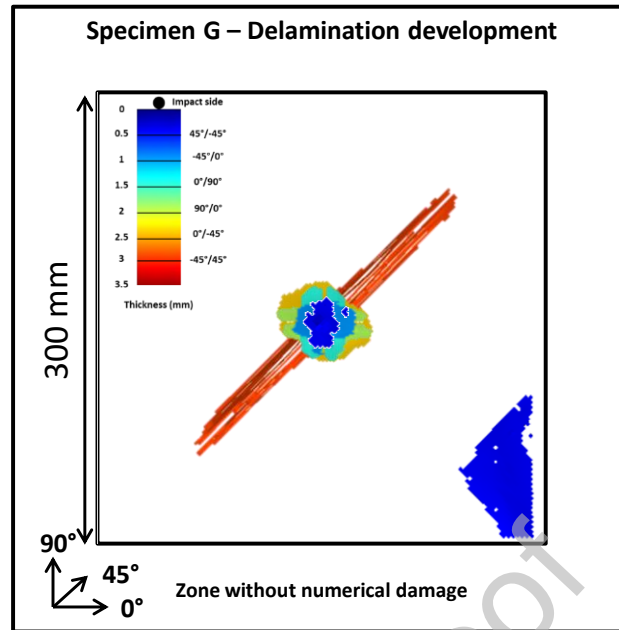


Figure 27: Delamination evolution during the loading after impact for specimen G

Compression (specimen G)

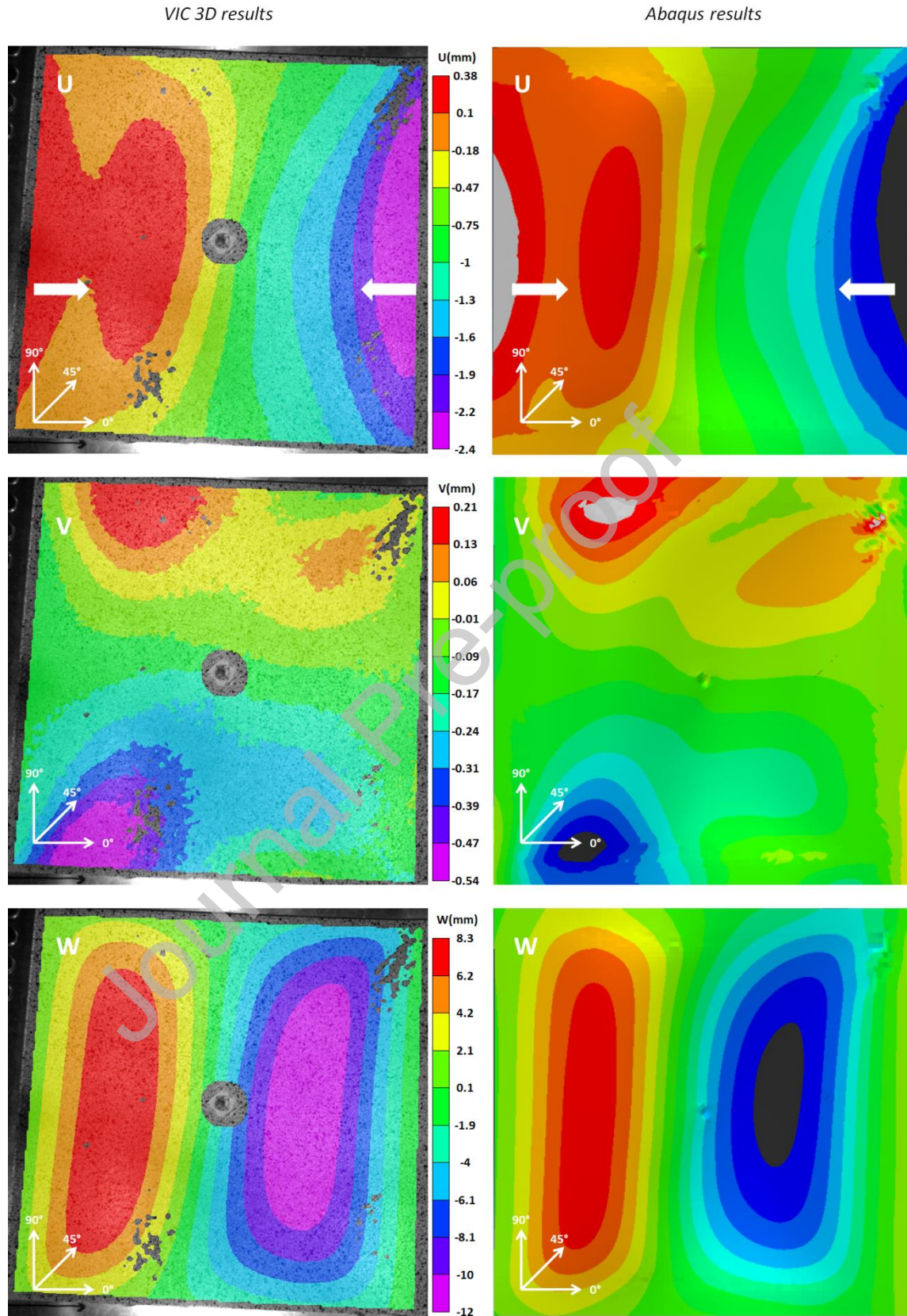


Figure 28: Experimental and DPM displacement fields in compression just before failure

Synthesis

Figure 29 represents the numerical and experimental loading paths for specimens A, B, C, F and G in terms of averaged stress and global strains.

With the exception of specimens C and F in the global strains graph, the loading path of each specimen up to final failure is very well represented with the DPM. The DPM is efficient to capture the buckling and the associated buckling modes but sometimes leads to an earlier failure. The DPM shows its capabilities as far as studying the interaction between the delaminated area after impact and the structure postbuckling is concerned. As estimated in [51], damage induced by the impact has little influence on the post-buckling failure except in specimen F. Final failure profiles are also well modeled and the DPM proves to be useful to study the failure initiation and propagation.

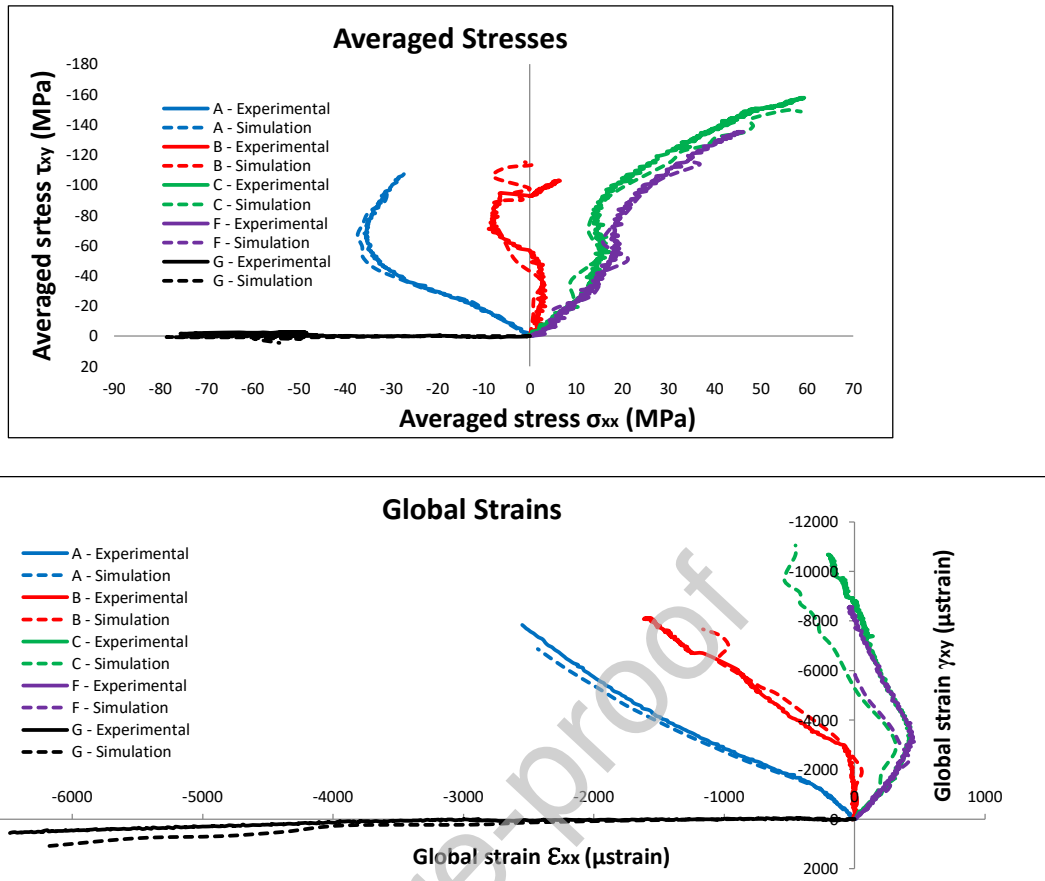


Figure 29: Comparison of numerical and experimental loading paths in terms of global strains and averaged stresses

4. Conclusion

In this paper, the DPM was used to simulate VERTEX tests described in [51]. The objective of DPM simulations is to be able to answer a few questions regarding the location of the failure initiation and the interaction between impact damage and postbuckling behavior.

The first step was to validate DPM capabilities to simulate medium velocity impact, from 54 m/s to 110 m/s, on large composite laminate plates. Thanks to a numerical/experimental comparison of force versus impactor displacement curves and delaminated areas obtained with C-scan, this first step was successfully validated.

The second step was to simulate complex loading after the impact. Boundary conditions recovered from DIC were applied to the DPM with the method validated using an implicit model without any damage representation [51]. In order to implement these boundary conditions, the plate was meshed in three parts: one with damageable volume elements used with DPM behavior laws, one with volume elements (1 per ply) used as a transition zone and one external part with one non-damageable thick shell element in the plate thickness. This configuration allowed the authors to use exactly the same boundary conditions as those used in the simplified mode in [51]. Five specimens were studied in this work: specimen A in compression/shear loading (impacted at 54m/s), specimen B in pure shear loading (impacted at 70 m/s), specimens C and F in tension/shear loading (respectively impacted at 75 m/s and 100 m/s) and specimen G in pure compression (impacted at 110 m/s).

DPM simulations gave good results in all types of loading. Tension/shear behaviors could be improved since the buckling points appeared too early in the simulations. The post-buckling behaviors were therefore influenced and diverged slightly from the experimental ones. The

discrepancy between numerical and experimental results can probably be explained by the quality of the boundary conditions extracted from the experimental data (from stereo-correlation) and implemented in the model. For the present study, the shape of the plate once bolted to the test bench was not taken into account in the numerical model. In other words, the experimental boundary conditions were applied to a perfectly flat plate whereas the experimental observations show that, after this bolting operation, some loading is already applied to the specimen, which deforms accordingly. This initial small curvature should have some influence on the global behavior, especially when loading (compression or shear) triggers buckling. Additionally, it should be mentioned that displacements used as boundary conditions were applied to both the top and the bottom surface of the plate. To be efficient, it would be necessary obtain the rotation of the plate through different displacements applied to the top and the bottom surfaces. Research is still on-going to assess the influence that the type of boundary conditions used in a numerical model has on the correlation with experimental data.

In most cases, the DPM confirms the location of the failure occurrence observed experimentally. Except for specimen B, the failure appears first in the plate bottom right corner and then propagates to the top left corner through the impact mark. This also makes it possible to show that the delaminated area after impact was not propagated during the loading after impact. This behavior seems to indicate that the impact damage does not play a predominant role in the final failure.

The DPM gave encouraging results for simulating the medium velocity impact and the complex loading after impact in the same model. The implementation of boundary conditions in an explicit scheme must be investigated if a better correlation between

numerical and experimental results is to be obtained. Finally, computation times associated with such simulations are too long (50 h with 36 CPUs). This last point needs to be improved before industrial use of the DPM can be envisaged.

Damage from the impact had little influence on the post-buckling failure except for specimen B. This result is very interesting because it contradicts the classical results of the literature [5-6]. It is noteworthy that the energy involved in the present study (from 40.8 J to 169.4 J) is very high compared with the classical ones (around 50 J). These conflicting results should be explained by the size of the specimen. The standard tests of impact and compression after impact [7-8] are performed on small coupons of $100 \times 150 \text{ mm}^2$; which induces greater impact damage (for a given impact energy) and, at the same time, a larger zone of impact damage relatively to the coupon size. The present study shows that, for larger specimens, the impact damage is less prevalent and decreases the residual strength less. In fact, the buckling mode clearly affects the final failure more than the impact damage does. This result stresses the interest of the pyramid of tests design philosophy [14], even though its benefit is already very clear in the industry.

In conclusion, the pyramid of tests design is clearly a crucial point of composite structure design, and test rigs, such as the VERTEX machine [66], able to evaluate the residual strength after impact on a real structure, or at least at the level 2 of the pyramid of tests [14] are, more than ever, needed to avoid oversizing composite structures.

Acknowledgements

The authors gratefully acknowledge CALMIP (CALcul en Midi-Pyrénées, (<https://calmip.univ-toulouse.fr>) for access to the HPC resources under the allocation p1026.

References

- [1] E. Morteau, C. Fualdes. Composites @ Airbus, Damage Tolerance Methodology. FAA Workshop for Composite Damage Tolerance and Maintenance, Chicago IL, 2006
- [2] N. Dubary, C. Bouvet, S. Rivallant, L. Ratsifandrihana. Damage tolerance of an impacted composite laminate. *Composite Structures*, 206: 261-271, 2018
- [3] S. Abrate. *Impact on Composite Structures*. Cambridge University Press, 1998
- [4] P. Perugini, A. Riccio, F. Scaramuzzino. Influence of delamination growth and contact phenomena on the compressive behavior of composite panels. *Journal Of Composite Materials*, 33(15) : 1433-1456 ,1999
- [5] A. Tropis, M. Thomas, J.L. Bounie, P. Lafon. Certification of the composite outer wing of the ATR72. *Journal of Aerospace Engineering, Proceedings of the Institution of mechanical Engineers Part G*, 209 : 327-339, 1994
- [6] G. Caprino, V. Lopresto. The significance of indentation in the inspection of carbon fibre-reinforced plastic panels damaged by low-velocity impact. *Composites Science and Technology*, 60 : 1003-1012, 2000
- [7] ASTM D7136/D7136M. Standard Test Method for Measuring the Damage Resistance of a Fiber-Reinforced Polymer Matrix Composite to a Drop-Weight Impact Event, 2015
- [8] ASTM D7137/D7137M. Standard Test Method for Compressive Residual Strength Properties of Damaged Polymer Matrix Composite Plates, 2012
- [9] G. Zhou. The use of experimentally-determined impact force as damage measure in impact damage resistance and tolerance of composite structures. *Composite Structures*, 42:375–82, 1998

- [10] H. Suemasu, T. Kumagai, K. Gozu. Compressive behavior of multiply delaminated composite laminates part 1: experiment and analytical development. *AIAA J*, 36(7):1279–85, 1998
- [11] H. Suemasu, T. Kumagai. Compressive behavior of multiply delaminated composite laminates part 2: finite element analysis. *AIAA J*, 36(7):1286–90, 1998
- [12] R. Olsson. Analytical prediction of large mass impact damage in composite laminates. *Compos A*, 32:1207–15, 2001
- [13] K.Y. Huang, A. De Boer, R. Akkerman. Analytical modeling of impact resistance and damage tolerance of laminated composite plates. *AIAA J*, 46(11):2760–72, 2008
- [14] J. Rouchon. Certification of Large Aircraft Composite Structures, Recent Progress and New Trends in Compliance Philosophy, presented at the 17th ICAS, Stockholm, Sweden, 1990
- [15] Q.D. Yang, B.N. Cox, X.J. Fang, Z.Q. Zhou. Virtual Testing for Advanced Aerospace Composites: Advances and Future Needs. *Journal of Engineering Material and Technology*, 133(1):011002, 2011
- [16] C.S. Lopes, P.P. Camanho, Z. Gurdal, P. Maimi, E.V. Gonzalez. Low-Velocity impact damage on dispersed stacking sequence laminates. Part II: Numerical simulations. *Composites Science and Technology*, 69(7-8): 937-947, 2009
- [17] C.S. Lopes, S. Sadaba, C. Gonzalez, J.L. Lorca, P.P. Camanho. Physically-sound simulation of low-velocity impact on fiber reinforced laminates. *Int J Impact Eng*, 92:3–17, 2015
- [18] M.R. Wisnom. Modelling discrete failures in composites with interface elements. *Composites Part A: Applied Science and Manufacturing*, 41(7): 795-805, 2010
- [19] C. Menna, D. Asprone, G. Caprino, V. Lopresto, A. Prota. Numerical simulation of impact tests on GFRP composite laminates. *Int J Impact Eng*, 38:677–85, 2011

- [20] P. Zafer Kutlu, F.-K. Chang. Modeling Compression failure of laminated Composites Containing multiple through-the-width delaminations. *Journal of Composite Materials*, 26: 350-387, 1992
- [21] Z. Aslan, M. Sahin. Buckling behaviour and compressive failure of composite laminates containing multiple large delaminations. *Composite Structures*, 89:382–90, 2009
- [22] T.D. Dang, S.R. Hallett. A numerical study on impact and compression after impact behavior of variable angle tow laminates. *Composite Structures*, 96: 194-206, 2013
- [23] H.Y. Choi, F.K. Chang. A model for predicting damage in graphite/Epoxy laminated composites resulting from low-velocity point impact. *Journal of Composite Materials*, 26(14): 2134-2169, 1992
- [24] R. Krueger. The virtual crack closure technique: history, approach and applications. NASA/Contractor Report-2002-211628, 2002
- [25] S. Li, S.R. Reid, Z. Zou. Modelling damage of multiple delaminations and transverse matrix cracking in laminated composites due to low velocity lateral impact. *Composites Science and Technology*, 66: 827-836, 2006
- [26] D.S. Dugdale. Yielding of steel sheets containing slits. *J. Mech. Phys. Solids*, 8: 100-108, 1960
- [27] G.I. Barenblatt. The mathematical theory of equilibrium of cracks in brittle fracture. *Adv. Appl. Mech.*, 7: 55-129, 1962
- [28] A. Faggiani, B.G. Falzon. Predicting low-velocity impact damage on a stiffened composite panel. *Composites Part A: Applied Science and Manufacturing*, 41(6): 737-749, 2010
- [29] Y. Shi, T. Swait, C. Soutis. Modelling damage evolution in composite laminate subjected to low velocity impact. *Composite Structures*, 94(9): 2902-2913, 2012

- [30] F. Aymerich, F. Dore, P. Priolo. Prediction of impact-induced delamination in cross-ply composite laminates using cohesive interface elements. *Composites Science and Technology*, 68: 2383-2390, 2008
- [31] X.C. Sun, M.R. Wisnom, S.R. Hallet. Interaction of inter-and intralaminar damage in scaled quasi-static indentation tests: Part 2 –Numerical simulation. *Composite Structures*, 136: 727-742, 2016
- [32] A. Turon, C.G. Dávila, P.P. Camanho, J. Costa. An engineering solution for mesh size effects in the simulation of delamination using cohesive zone models. *Engineering Fracture Mechanics*, 74(10): 1665-1682, 2007
- [33] P.W. Harper, L. Sun, S.R. Hallett. A study on the influence of cohesive zone interface element strength parameters on mixed mode behavior *Composites Part A:Applied Science and Manufacturing*, 43 : 722-734, 2012
- [34] Z. Ji, Z. Guan, Z. Li. A progressive damage model for predicting permanent indentation and impact damage in composite laminates. *Applied Composite Materials*, 1-20, 2016
- [35] M.V. Donadon, L. Iannucci, B.G. Falzon, J.M. Hodgkinson, S.F.M. de Almeida. A progressive failure Model for composite laminates subjected to low velocity impact damage. *Computers and Structures*, 86: 1232-1252, 2008
- [36] P. Maimi, P.P. Camanho, J.A. Mayugo, C.G. Davila. A continuum damage model for composite laminates: Part I –Constitutive model. *Mechanics of Material*, 39: 897-908, 2007
- [37] Z. P. Bazant, B. H. Oh. Crack band theory for fracture of concrete. *Materials and Structures*, 16: 155 – 177, 1983

- [38] S.T. Pinho, P. Robinson, L. Iannucci. Fracture toughness of tensile and compressive fibre failure modes in laminated composites. *Composites Science and Technology*, 66: 2069-2079, 2006
- [39] C. Bouvet, S. Rivallant, J.J. Barrau. Low velocity impact modeling in composite laminates capturing permanent indentation. *Composites Science and Technology*, 72: 1977-1988, 2012
- [40] M.F.S.F. de Moura, J.P.M. Gonçalves. Modelling the interaction between matrix cracking and delamination in carbon–epoxy laminates under low velocity impact. *Composites Science and Technology*, 64: 1021-1027, 2004
- [41] C. Bouvet, B. Castanié, M. Bizeul, J.J. Barrau. Low velocity impact modelling in laminate composite panels with discrete interface elements. *Int J Solids Struct*, 46(14–15):2809–21, 2009
- [42] C. Leopold, S. Harder, C. Buggish, W.V. Leibig, B. Fiedler. Influence of 90° layer thickness on damage initiation and propagation in CFRP cross ply laminates. 17th European Conference on Composite Materials, Germany, 2016
- [43] L. Lammerant, I. Verpoest. Modelling of the interaction between matrix cracks and delaminations during impact of composite plates. *Composites Science and Technology*, 56(10): 1171-1178, 1996
- [44] E.V. Iarve, M.R. Gurvich, D.H. Mollenhauer, C.A. Rose, C.G. Davila. Mesh-independent matrix cracking and delamination modeling in laminated composites. *Int J Numer Methods Eng*, 88:749–73, 2011

- [45] S.R. Hallett, W.G. Jiang, B. Khan, M.R. Wisnom. Modelling the interaction between matrix cracks and delamination damage in scaled quasi-isotropic specimens. *Composites Science and Technology*, 68(1): 80-89, 2008
- [46] E.V. Gonzalez, P. Maimi, P.P. Camanho, A. Turon, J.A. Mayug. Simulation of dropweight impact and compression after impact tests on composite laminates. *Compos Struct*, 91(11):3364–78, 2012
- [47] W. Tan, B.G. Falzon, L.N.S. Chiu, M. Price. Predicting low velocity impact damage and Compression-After-Impact (CAI) behavior of composite laminates. *Composites Part A: Applied Science and Manufacturing*, 71: 212-226, 2015
- [48] E. Panettieri, D. Fanteria, F. Danzi. Delamination growth in compression after impact test simulations: Influence of cohesive elements parameters on numerical results. *Composite Structures*, 137: 140-147, 2016
- [49] F. Caputo, A. De Luca, R. Sepe. Numerical study of the structural behaviour of impacted composite laminates subjected to compression load. *Composites Part B: Engineering*, 79: 456-465, 2015
- [50] M.R. Abir, T.E. Tay, M. Ridha, H.P. Lee. Modelling damage growth in composites subjected to impact and compression after impact. *Composite Structures*, 168: 13-25, 2017
- [51] A. Trellu *et al.*, 'Combined loadings after medium velocity impact on large CFRP laminate plates: Tests and enhanced computation/testing dialogue', *Compos. Sci. Technol.*, vol. 196, p. 108194, Aug. 2020, doi: 10.1016/j.compscitech.2020.108194.

- [52] B. Castanié, J.J. Barrau, J.P. Jaouen. S. Rivallant. Combined shear/compression structural testing of asymmetric sandwich structures. *Experimental Mechanics*. 44(5):461-472. 2004
- [53] J. Serra, J.E. Pierrié, J.C. Passieux, J.N. Périé, C. Bouvet, B. Castanié. Validation of aeronautical composite structures under multiaxial loading: the VERTEX Project. Part 1: Experimental Setup, Instrumentation with FE-SDIC and Procedures. *Composite Structures*, 179 : 224-244, 2017
- [54] G. Romeo, G. Frulla, Buckling and Post-buckling Behavior of Anisotropic Plates under Combined Biaxial Compression and Shear Loads, *ECCM Composite Testing and Standardization*, Amsterdam, 1992.
- [55] K. Wolf, H. Kossira, An Efficient Test Method for the Experimental Investigation of the Post-buckling Behavior of Curved Shear Panels, *ECCM Composite Testing and Standardization*, Amsterdam, 1992.
- [56] M. Rouse, R.D. Young, R.E. Gehrki, Structural Stability of a Stiffened Aluminum Fuselage Panel Subjected to Combined Mechanical and Internal Pressure Loads, 2003, p. 1423. AIAA Paper.
- [57] A. Bergan, J.G. Bakuckas, A. Lovejoy, D. Jegley, K. Linton, G. Korkosz, J. Awerbuch, T.M. Tan, Full-scale test and analysis of a PRSEUS fuselage panel to assess damage-containment features, in: *Aircraft Airworthiness & Sustainment Conference*, 2011. San Diego, California, April 18-21, 2011.
- [58] R.W. Peters. Buckling tests of flat rectangular plates under combined shear and longitudinal compression. *NACA Tech. Note 1750*, 1948.

- [59] H. Klein, General about buckling tests with thin-walled shells, Rap. DLR- Mitt 89–13 (1989).
- [60] G. Zucco, V. Oliveri, D. Peeters, R. Telford, G.J. Clancy, C. McHale, M. Rouhi, R. O'Higgins, M.R. Young, P.M. Weaver, Static test of a thermoplastic composite wingbox under shear and bending moment, in: 2018 AIAA/ASCE/AHS/ASC Structures, Structural Dynamics, and Materials Conference 8–12 January 2018 Kissimmee, 2018, <https://doi.org/10.2514/6.2018-0482>. Florida.
- [61] B. Castanié, J.J. Barrau, J.P. Jaouen. Theoretical and experimental analysis of asymmetric sandwich structures. *Composite Structures*, 55(3):295-306, 2002
- [62] J. Serra, J.E. Pierrié, J.C. Passieux, J.N. Périé, C. Bouvet, B. Castanié, C. Petiot. Validation of aeronautical composite structures under multiaxial loading: the VERTEX Project. Part 2: Load envelopes for the assessment of panels with large notches. *Composite structures*, 180: 550-567, 2017
- [63] S. Rivallant, C. Bouvet, N. Hongkarnjanakul. Failure analysis of CFRP laminates subjected to compression after impact: FE simulation using discrete interface elements. *Composites Part A: Applied Science and Manufacturing*, 55 : 83-93, 2013
- [64] J. Serra, C. Bouvet, B. Castanié, C. Petiot, Scaling effect in notched composites: the Discrete Ply Model approach, *Compos. Struct.* 148 (2016) 127–143, <https://doi.org/10.1016/j.compstruct.2016.03.062>.
- [65] J. Serra, C. Bouvet, B. Castanié, C. Petiot, 'Experimental and Numerical Analysis of Carbon Fiber Reinforced Polymer Notched Coupons under Tensile Loading'. *Composite Structures* 181 (December): 145–57. <https://doi.org/10.1016/j.compstruct.2017.08.090>.

[66] <http://www.institut-clement-ader.org/vertex/>

[67] Abaqus 2016 Analysis user's manual, Dassault Systemes Simulia, 2016

[68] <http://www.institut-clement-ader.org/plateformes/stimpact/>

[69] J.-E. Pierré, J.-C. Passieux, J.-N. Périé. Finite Element Stereo Digital Image Correlation: framework and mechanical regularization. *Experimental Mechanics*. Online, 1-14. 2017

Declaration of interests

☒ The authors declare that they have no known competing financial interests or personal relationships that could have appeared to influence the work reported in this paper.

☐ The authors declare the following financial interests/personal relationships which may be considered as potential competing interests:

--